1. Application of a Focussed Ion Beam (FIB) system to biological samples

This chapter describes the working principles of Focussed Ion Beam (FIB) system. It demonstrates that it is a powerful tool for the investigation of biological materials. Its combination of a microscope with a large depth of focus with a cutting tool for the site-specific and precise preparation of cross-sections offers excellent new opportunities for the investigation of the structure and geometry of samples in the micrometer range. After a literature review in Chapter 1.2 and first applications of the FIB on biological structures in Chapter 1.3, systematic investigations of the interactions of the ion beam with biological materials and the effects of the Ga^+-ions on its structure and mechanical properties, such as the rise in temperature due to the ion beam and the change in the mechanical properties are described in Chapter 1.6.3 and 1.6.4 respectively. In Chapter 1.7, the advantages and disadvantages of various FIB techniques such as imaging, milling and gas deposition are discussed in the context of the literature published so far.

1.1 Introduction: The Focussed Ion Beam (FIB) system

A Focussed Ion Beam microscope (FIB) operates in principle like a scanning electron microscope (SEM). A fine electron beam is made to scan the sample point by point on a raster. Secondary (or backscattered) electrons produced at each point are collected, with suitable electronics to produce an image on a computer screen in synchronism with the scanning beam. A FIB system differs from an SEM in that it uses an ion beam (commonly Ga^+-ions) instead of an electron beam to create secondary electrons and ions for imaging. The Ga^+-ions are extracted from a liquid-metal ion source (LMIS) by an applied electric field. An electromagnetic lens system forms the ions to a beam and rasters it over the sample. The whole system operates in vacuum to prevent the ions from any interactions with any other ions or molecules.

A FIB system is, like an SEM, a tool for high resolution microscopy, with a spatial resolution of typically 6 nm. The advantage of the FIB system over an SEM is that, in addition to imaging, its ion beam can be used as a cutting tool with a spatial resolution of a cut of about 10 nm. By scanning the ion beam several times over a defined area, the interaction of the highly accelerated ions cause the atoms and ions at the sample surface to be sputtered away (milled). To mill large volumes, Gas Assisted Etching systems (GAE) can be used. A GAE

system injects a precursor gas, which interacts with the ion beam to form free radicals (fluoride or chloride) or water (selective carbon milling), into the specimen chamber. These free radicals etch the sample at a well defined region, where the ion beam scans the sample surface. However, the FIB cannot only be used to remove material, it can also be used to deposit material using the Gas Assisted Deposition (GAD) system. This system works similar to the GAE system with a so called precursor gas. It is cracked by the ion-beam to form a metal or insulator (typically W, Pt or SiO_2). The volatile part is removed by the pumping system of the FIB.

Several parameters influence the imaging, milling and GAD performance. These are the beam current, the dwell time and the overlap. The beam current is the amount of ion current striking the sample, the dwell time is the time that the beam remains at one given position (pixel, typically 1 μs) and the overlap defines the percentage of beam overlap between adjacent positions (pixels) when the beam is scanned across the sample.

Since their development in the early 1980s, FIB systems have become well established tools in the semiconductor industry as a device to micro-machine and repair semiconductor photo-masks (e.g. Phaneuf, 1999). More recently FIBs are increasingly being used in materials science as a tool for imaging and site-specific micromachining, so far mainly for metals and ceramics.

Already a relatively new tool in materials research, the FIB has been applied even less to biological samples. Chapter 1.2 reviews the literature published so far on the use of the FIB system for the investigation of biological materials.

1.2 Literature review: FIB investigations on biological materials

Comparatively little experience exists with the use of FIB systems for the investigation of biological and polymeric materials, a fact which is reflected in the relatively small number of publications on this topic. Table 1.1 gives an overview of the publications concerning the use of ion etching and FIB systems for the investigation of biological and polymeric materials. It lists, in chronological order, the author, the sample material and beam conditions used, as well as the application for which the sample was made.

Table 1.1: Summary of the literature published, in chronological order, concerning the use ion etching and FIB techniques for the investigation of biological or polymeric materials.

Reference	**Material**	**Type of ions**	**Voltage**	**Beam current**	**Use**
Lewis *et al.* 1968	Blood cell	Ion etching using Ar, H, O and H_2O vapour			SEM
Yonehara *et al.* 1989	Mouse microvilli	Ga	2 kV	60 µA	FE-SEM
Kanaya *et al.* 1992	Human tooth enamel and dentine, microvilli and rat liver	A^+-ion beam etching	2-5 kV		SEM
Young *et al.* 1993	Mites	Ga, spot size ~ 50 nm		34-64 pA (milling)	SEM
Mackenzie *et al.* 1993	Eye of a housefly	Ga, spot size 250 nm (milling)	25 kV		FIB
van Meerbeek *et al.* 1995	Resin-dentin interface	Ga			FIB
Ishitani *et al.* 1995	Human hair eye of a housefly	Ga	30 kV	<100 pA	FIB
Ballerini *et al.* 1997	Yeast cells	Ga			FIB
Duane 1997	Palynological material	Ga, spot size 20-400 nm	30 kV	750 pA (milling), 100 pA (cleaning)	FIB
Ballerini *et al.* 1998	Yeast cells	Ga			FIB
Batani *et al.* 1998	Yeast cells	Ga			FIB
Hayashi *et al.* 1998	Human enamel	Ga			HRTEM
Milani *et al.* 2000	Yeast cells	Ga			FIB
Ballerini *et al.* 2001	Yeast cells	Ga	30 kV	10 pA (milling)	FIB
Hoshi *et al.* 2001	Human dentin	Ga, spot size 50-800 nm	30 kV	12 nA (milling), 50 pA (trimming)	EF-TEM
Suzuki *et al.* 2001	Marine diatom	Ga			
Aubry *et al.* 2002	PMMA, polyimide	Ga, spot size >1µm	12 kV, 26 kV		
Volkert *et al.* 2004	Fluorapatite-gelatine composite particles	Ga	30 kV		TEM
Drobne *et al.* 2005	Digestive gland cells of *Porcellio scaber*	Ga, spot size 50-300 nm	30 kV	5-7 nA (milling), 0.3-1.0 nA (cleaning)	FIB, SEM
Milani *et al.* 2005	Digestive gland cells of *Porcellio scaber*	Ga	30 kV	5-7 nA (milling), 0.3-1.0 nA (cleaning)	FIB, SEM
Burkhardt *et al.* 2005	Osteoblast and fibroblast cells	Ga			FIB, SEM
Gnauck *et al.* 2005	Fibroblast cells	Ga			FIB, SEM, STEM

In the following, the literature concerning the use of the FIB or other ion etching systems is reviewed in detail.

- Lewis *et al.* (1968) investigated human blood cells in an SEM after ion etching using argon, hydrogen, oxygen and water vapour.
- Yonehara *et al.* (1989) investigated argon ion beam etching of mouse microvilli (cells covering the small intestine). The authors studied the topographic specimen characteristics by etching the longitudinal side of the microvilli.
- Kanaya *et al.* (1992) analysed quantitatively the sputtering due to ion beam bombardment of solids and biological specimens. The biological specimens observed were human tooth enamel and dentine, microvilli of the small intestine and a freeze-fractured surface of a rat liver.
- Young *et al.* (1993) investigated ion beam milling for the internal morphology of the respiratory system of mites of the family *Halarachnidae* (*Mesostigmata: Acarina*) and of sensory of the setae sensory organ, called Haller´s organ. A series of square holes were milled perpendicular to the cuticular surface to expose the internal features of the peritreme (a fold of the cuticle).
- Mackenzie *et al.* (1993) prepared cross-sections of an eye of a housefly.
- Van Meerbeek *et al.* (1995) demonstrated the FIB cross-sectioning technique for ultra-structural examination of resin-dentin interfaces.
- Ishitani *et al.* (1995) investigated the focussed ion beam milling techniques for biological samples, such as human hair and the eye of a housefly.
- Duane (1997) prepared cross-sections of Palynomorphs (organic-walled microfossils, mainly from pollen or spores).
- The FIB can be used for the investigation of cells, which was demonstrated on *Saccharomyces cerevisiae* yeast cells. The tree dimensional constitution, the topography and the interior of yeast cells was investigated without further sample preparation (Ballerini *et al.,* 1997; Ballerini *et al.,* 1998; Batani *et al.,* 1998; Milani *et al.,* 2000; Ballerini *et al.,* 2001).
- Hayashi *et al.* (1998) prepared samples for high resolution transmission electron microscopy (HRTEM) out of two human mandibular third molars using the FIB. The samples were immersed, fixed with osmium tetroxide and dehydrated.
- Hoshi *et al.* (2001) prepared a Transmission Electron Microscopy (TEM) lamella out of a human dentine.

- Suzuki *et al.* (2001) prepared cross-sections of marine diatoms using the FIB system.
- The FIB technique can also be used to micromachine polymer samples. Aubry *et al.* (2002) micromachined gratings of PMMA and a fluorinated polyimide using a FIB system.
- Volkert *et al.* (2004) used the FIB system for the site specific preparation of fluorapatite-gelatine composite particles TEM samples. The FIB system was used for the preparation of these brittle samples, because conventional fabrication techniques induced artefacts such as fractures.
- Drobne *et al.* (2005) and Milani *et al.* (2005) prepared cross-sections of digestive gland epithelium of *Porcellio scaber* (Isopoda, Crustacea) for SEM and FIB microscopy. The samples were fixated, dehydrated, critical point dried and gold sputtered.
- Burkhardt *et al.* (2005) and Gnauck *et al.* (2005) prepared cross-sections and STEM lamellae from Araldite embedded osteoblast and fibroblast cells, grown on hard substrates (titanium film deposited on silicon), using a FIB system. From the cross-sections they investigated the interface structure between cell and substrate.

The review of the literature published to date shows that FIB systems have, until now, mainly been used for the preparation of cross-sections. Standard system settings established for technical materials were used to mill a box shaped section into biological materials. The only more systematic use was the preparation of TEM lamella samples, from dentin and enamel (Hayashi *et al.,* 1998; Hoshi *et al.,* 2001; Volkert *et al.* 2004) and the preparation of cross-sections from embedded osteoblast and fibroblast cells grown on hard substrates (Burkhardt *et al.,* 2005; Gnauck *et al.,* 2005).

Lacking so far are quantitative investigations on the influence of the ion beam on the sample material and the determination of optimal parameters for the imaging and milling of biological materials. In the literature so far, authors discuss the major disadvantages of the FIB system, such as the damage of the sample due to irregular sputtering, a temperature rise and/or shrinkage of the biological material (Melngailis, 1987; Ishitani *et al.,* 1995; Ishitani and Kaga, 1995), mainly qualitatively.

1.3 Microscopy and milling of biological materials

The literature review showed that, to date, comparatively little is known about the behaviour of biological materials in the FIB and under the influence of a Ga^+-ion beam. This is investigated in more detail in the following sections.

1.3.1 Sample condition

The condition of a biological sample is important for two reasons, the applicability of the FIB for its investigation, and the structural and mechanical changes of the sample itself. For an investigation in the FIB, samples have to be dry mounted (air dry). One reason is to reduce the pumping-down time of the vacuum chamber. Another, that water, which evaporates during the pumping-down process, can react with precursor materials in the GAE systems to form harmful substances. A reaction of water with fluorine (from the XeF_2 gas in the enhanced etching mode of the GAE) would set free hydrofluoric acid, for example.

1.3.2 Imaging

Our preliminary investigations in the imaging mode of the FIB of a variety of air dry polymeric and mineralised biological materials, such as insect cuticle, wood, nut shells, egg shells and ivory, demonstrated that the system is well suited for the examination of biological specimens, mineralised and non-mineralised. It even has the advantage over SEMs that charging effects are much reduced due to the fact that Ga^+-ions are implanted into the sample surface, forming a conductive layer over which charges can be spread and reduced. Figure 1.1 shows an example of a FIB micrograph of insect cuticle, it shows some hairs on the back of a housefly (*Musca domestica*).

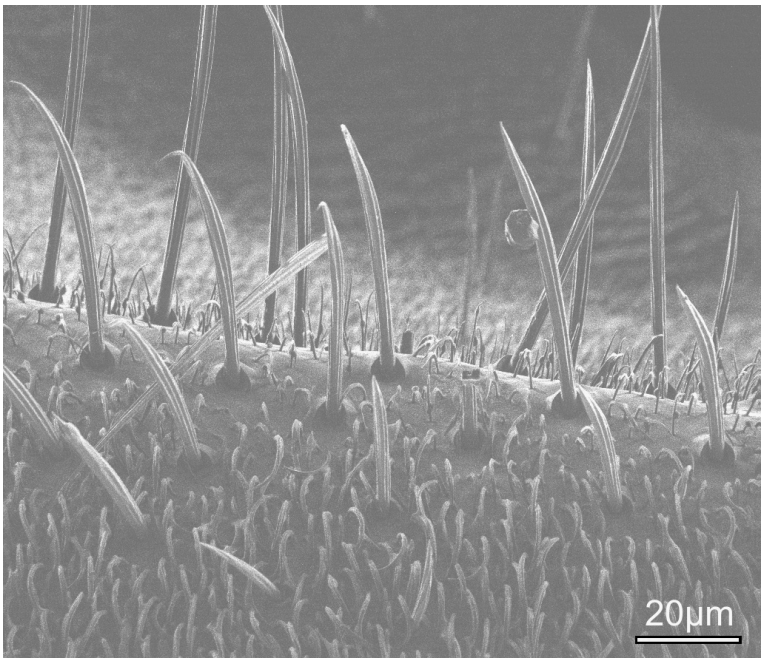

Figure 1.1: FIB micrograph of hairs on the back of a housefly (*Musca domestica*) (FIB micrograph).

Charging effects can be further reduced by coating the sample with a conductive layer, preferably one with a low sputter coefficient, such as carbon.

1.3.3 Milling

Since Ishitani *et al.* (1995) had demonstrated that it is possible to micromachine a small box into one segment of the fly's eye using the FIB, the eye of a housefly (*Musca domestica*) was chosen as the sample for a first experiment of ion-milling into insect cuticle. For milling, a dwell time of 1.0 µs and an overlap of 50 % were used. Optimal parameters for biological materials have not been reported in literature, so far.

After the first test with the eye of the housefly, also a keratin (feather) sample and a wood sample (spruce wood), and more complex structures of insect cuticle, the attachment system of a beetle and a filiform sensor on crickets, were used to demonstrate the suitability of the FIB system for the imaging and micromachining of biological materials. In all the samples a box was milled and a FIB micrograph was taken from the cross-section, as shown in Figure 1.2 a)-d).

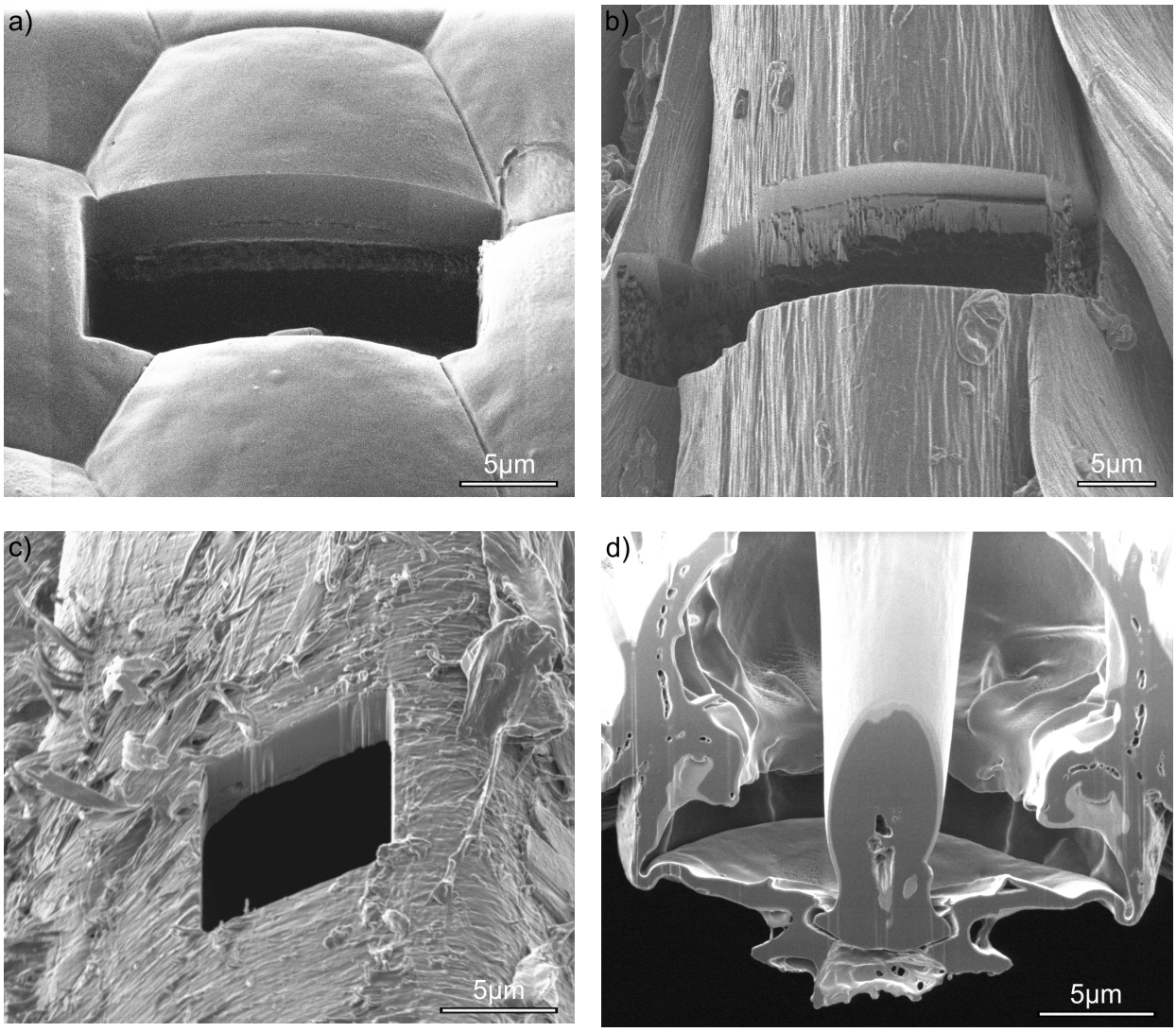

Figure 1.2: Cross-sections of milled boxes in a) an eye of a housefly, b) a feather, c) spruce wood cell wall and d) a filiform sensor on crickets (FIB micrographs; milling parameters: dwell time = 1.0 µs, overlap = 50 %).

1.4 Structural investigations using the FIB

The combination of a microscope with a milling tool allows to perform detailed investigations of complex biological structures in three dimensions. This is demonstrated on two different samples. Using the FIB system, cuts and cross-sections could be prepared site-specifically on samples in their natural state. This is not possible with any other preparation technique.

1.4.1 The hairy attachment system in insects

The splitting of the surface of the attachment pad into many fine contact points allows the foot of the beetle *Gastrophysa viridula* to conform to almost any surface, whether rough or smooth. Figures 1.3 and 1.4 are examples for the use of the FIB system for structural

investigations. Using a micromanipulator (MM3A, Kleindiek Nanotechnik), which is described in detail in Chapter 2.2, it was possible to bring a small piece of a silicon-oxide wafer in contact with the first attachment pad of the beetle. After a shear movement all setae were cut at half of their length, in order to investigate the arrangement of the individual setae in contact. Figure 1.3 shows the attachment procedure of the beetle foot on the surface. Figure 1.4 shows the cutting, the arrangement and the shape of the setae.

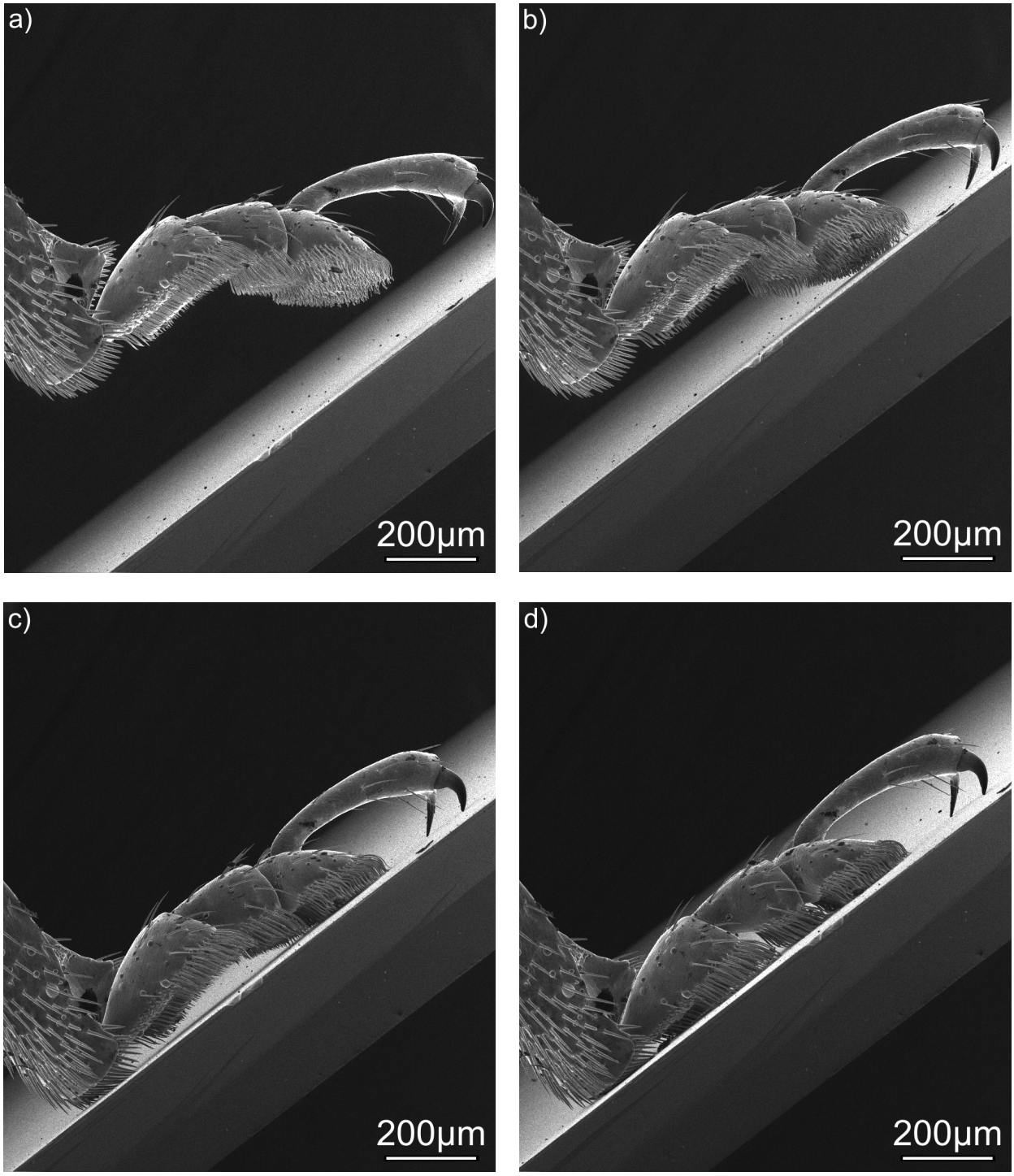

Figure 1.3: Attachment of the beetle's leg on a silicon oxide wafer
(FIB micrographs, milling parameters; beam current: 1000 pA, dwell time= 1.0 µs; overlap = 50 %).

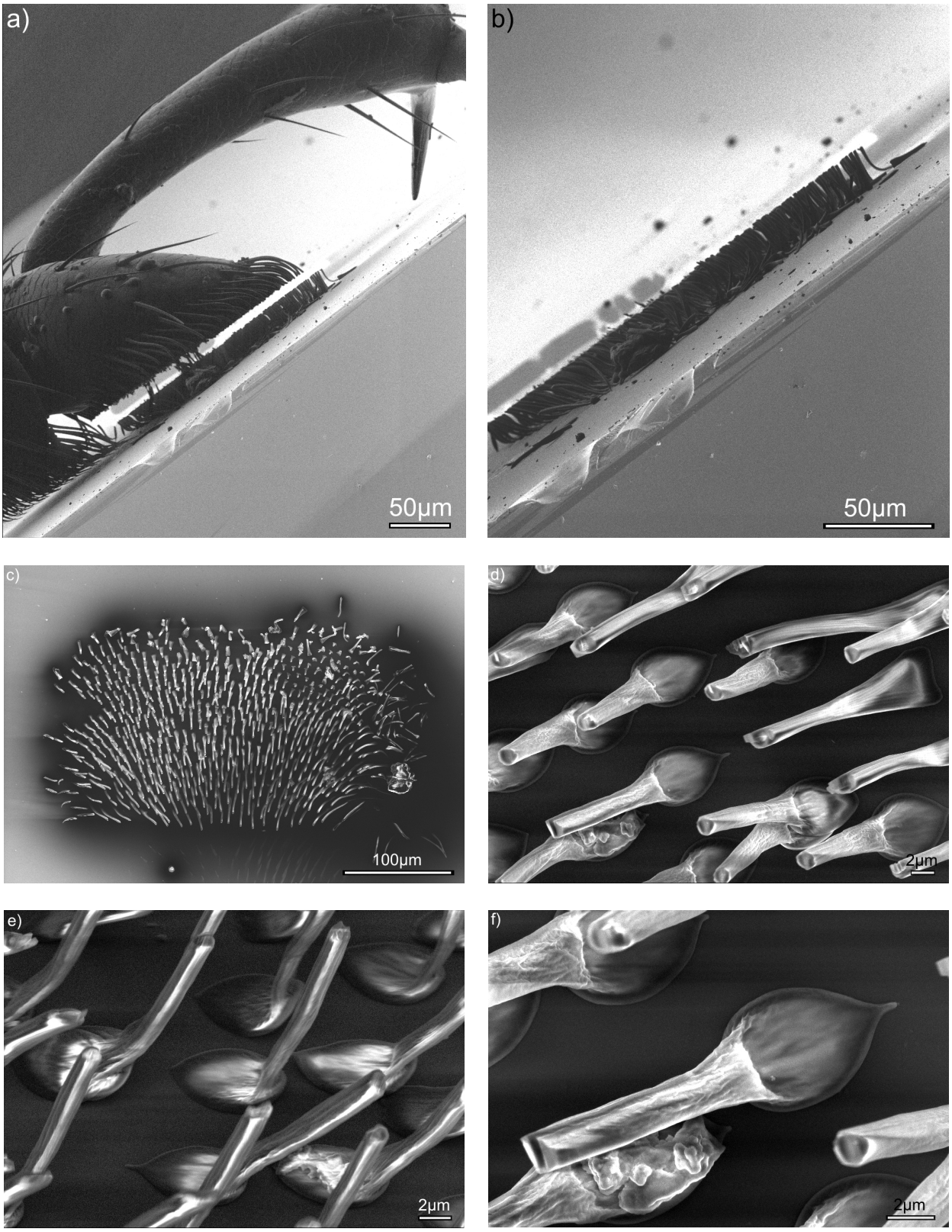

Figure 1.4: Arrangement of the setae in contact a) and b) are FIB and c) to f) are SEM micrographs; milling parameters: beam current = 1000 pA, dwell time = 1.0 µs, overlap = 50 %).

After the FIB system had been used simply for cutting, a more advanced procedure, the preparation of a high-precision cross-section of a complex structure was attempted.

1.4.2 Mechanoreceptors in insects

Insects have numerous mechanoreceptors which are sensitive to touch, air flow, sound, gravity and the deformation of the exoskeleton (Kiel, 1998). A number of cuticular structures serve as antennae for these stimuli and transfer mechanical stimulations to sensory cells positioned directly underneath the cuticle. The filiform sensors found on the cerci (the two sensory appendages found on the last abdominal segment, marked by a white arrow in Figure 1.5) of crickets, cockroaches and other insects are examples for this and have the function of an air flow sensor. Figure 1.5 shows an image of the cricket *Acheta domesticus*, the two cerci are marked by white arrows.

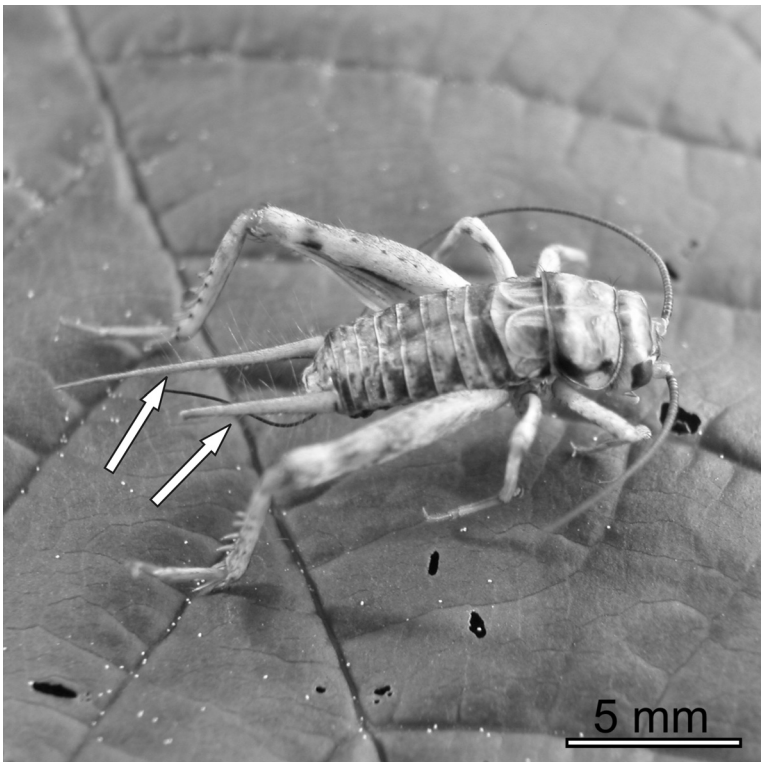

Figure 1.5: The cricket *Acheta domesticus*. White arrows mark the two cerci (Digital camera).

The filiform sensor consists of a wind-receptor hair which is tapered to the end and has a length ranging from 30 to 1500 µm and a diameter ranging from 1 to 9 µm on the cercus of adult crickets (Kamagai *et al.,* 1998). Under the influence of air flow, the hair deflects by an amount which is limited by the surrounding cup (Figure 1.6). The base of the hair forms a ball-and-socket joint at the bottom of the cuticular cup and is polar in construction so that deflection is possible in one plane only. At the base of the cup and in the plane of the hair movement, two circular structures, the so called campaniform sensilla, can be found. They are believed to detect the direction of the motion of the wind-receptor hair (Gnatzy and Schmidt,

1971). Figure 1.6 shows one of the filiform sensors found on the cerci of the cricket *Acheta domesticus*. The two arrows point to the campaniform sensilla.

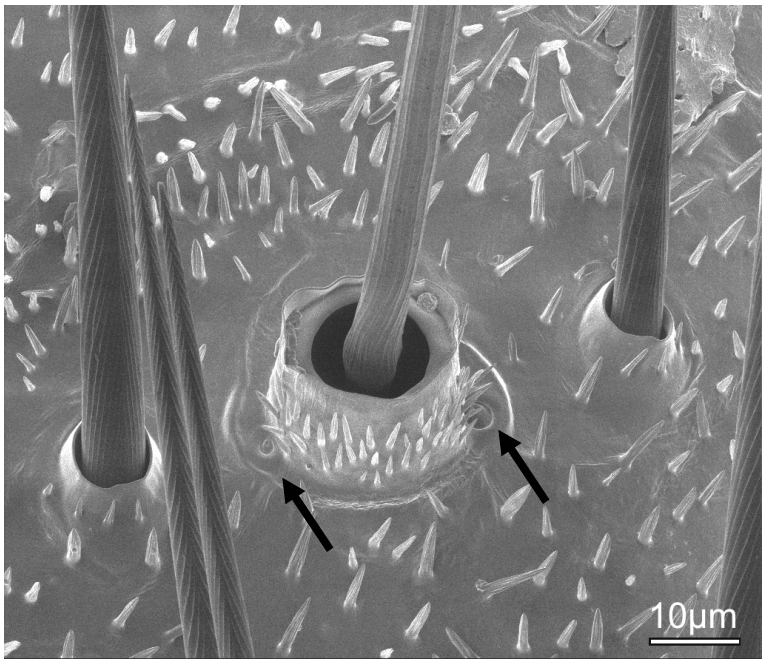

Figure 1.6: The base of the filiform sensor found on the cerci of the cricket *Acheta domesticus*. Black arrows mark the campaniform sensilla (FIB micrograph).

Filiform sensors of the cricket *Acheta domesticus* are an excellent example for a demonstration of the FIB as a powerful tool for the structural investigations of biological materials. Cross-sections were prepared on a sample that had been coated with a 6 nm thick gold-palladium layer in order to reduce charging effects. At first a box was milled close to the filiform sensor using a high beam current of 2700 pA. Afterwards, a cleaning process with a beam current of 70 pA was used in order to achieve a smooth cutting edge (dwell time = 1.0 µs, overlap = 50 %). Figure 1.7 shows the result, a cross-sectional view of the air-flow sensor, revealing its complex structure and geometry. For comparison Figure 1.8 shows an optical micrograph of a 500 to 1000 nm thick microtome section. The sample was dehydrated using ethanol, the ethanol was exchanged by resin, after hardening the embedded sample was cut into 500 to 1000 nm thick slices using a microtome, followed by standard preparation protocols for biological samples. Finally, the slices were stained using toluidine blue (Seidel, 2005).

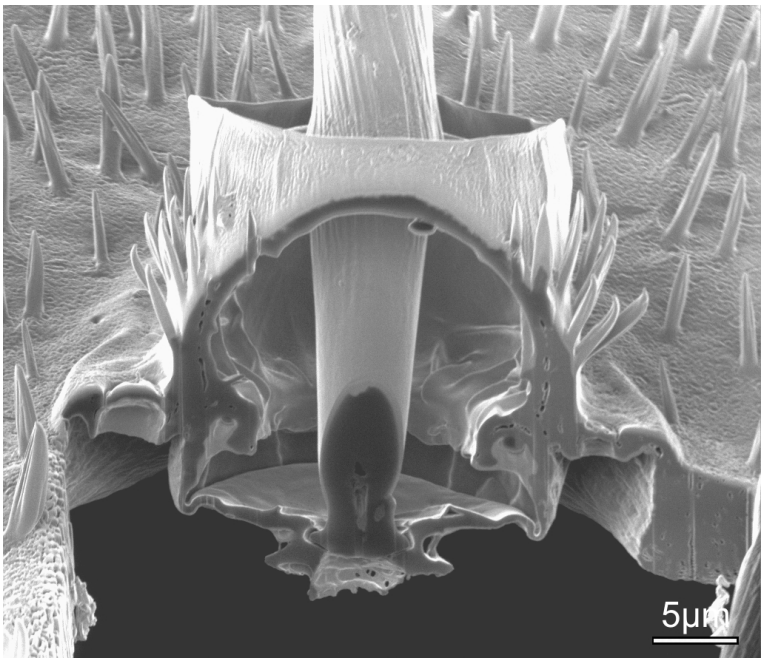

Figure 1.7: Cross-section of a filiform sensor found on the cerci of *Acheta domesticus* using the FIB system (FIB micrograph).

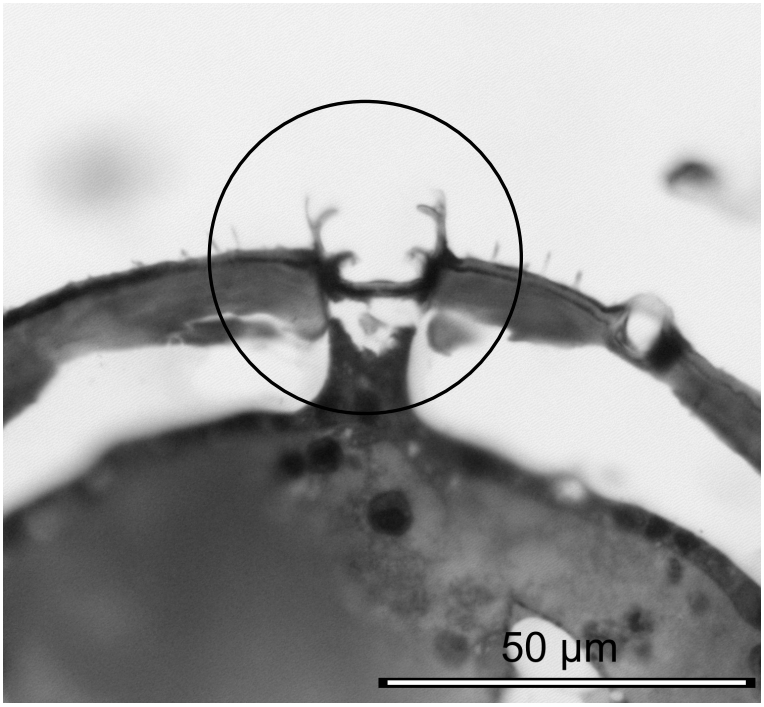

Figure 1.8: Cross-section of a filiform sensor found on the cerci of *Acheta domesticus* using conventional procedures for sample preparation (Optical micrograph, Seidel, 2005).

Figure 1.9 compares the two images. In both micrographs the base of the hair with the ball-and-socket joint at the bottom of the cuticular cup is visible.

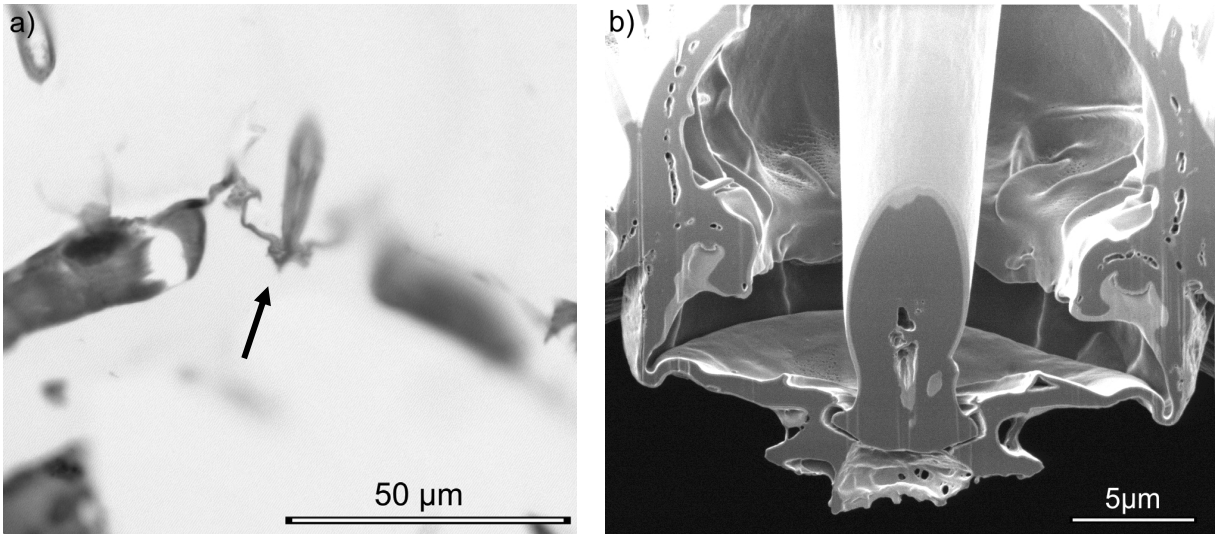

Figure 1.9: Cross-section of the ball-and-socket joint at the bottom of the wind-receptor hair:
a) obtained from conventional preparation techniques and optical microscopy
(Optical micrograph; Seidel, 2005), b) obtained using the FIB system (FIB micrographs).

Figure 1.7 demonstrates that the structure of the filiform sensor can be investigated in much greater detail using the FIB system. It provides a high precision milling technique which induces no mechanical damage due to cutting, like microtomes do, combined with high resolution microscopy, which is so far not achieved by any other technique.
Figure 1.10 shows a close-up of Figure 1.7 and reveals how the sensillum is connected to the circular cup and the hollow dome underneath.

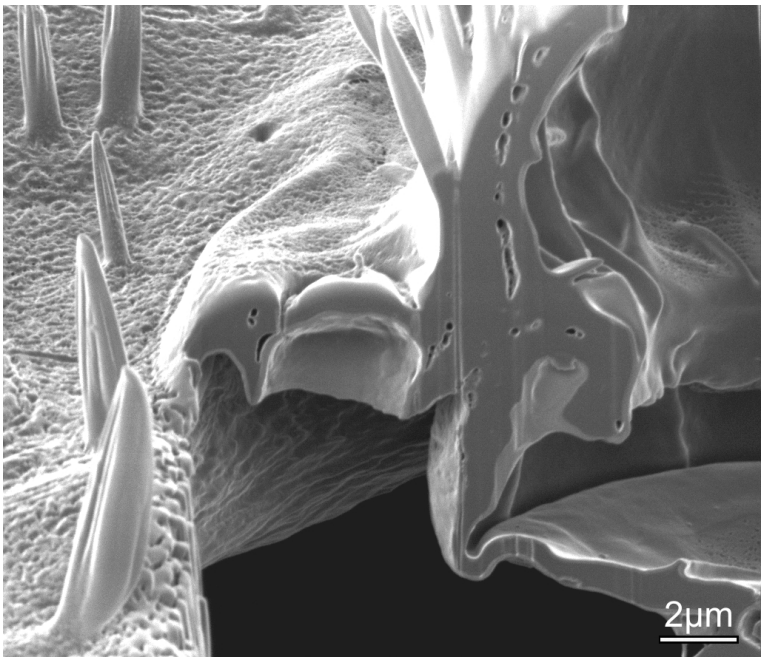

Figure 1.10: Cross-section of a campaniform sensillum (FIB micrograph).

The structural investigations of the hairy attachment system found in beetles and the filiform sensor were comparatively straight-forward applications of the FIB system for the exploration of complex, three-dimensional biological structures. The advantages of the FIB system for the investigation of 3-D structures are: (i) its large depth of focus combined with a topography and material contrast, (ii) the feasibility of site specific milling, (iii) the absence of artefacts due to mechanical sectioning of the sample, and (iv) the avoidance of elaborate sample preparation.

1.5 Milling process and sputter rate

Several parameters influence the ion beam milling process and within the sputter rates. These are the beam current, the dwell time, the overlap, the angle of incidence which is also correlated to the sample topography. The influence of these parameters on the milling performance on biological samples was investigated in detail.

1.5.1 Milling process

It is critical for an interpretation of the milled structure to know how the structure evolved during the milling process. This was investigated by milling a 7 µm × 7 µm × 3 µm box into the cuticle of the leg of the beetle *Pachnoda marginata*. A micrograph was taken every 30

seconds. The progress in the milling process is illustrated in Figure 1.11 by a subset of the micrographs taken.
Figure 1.11 shows phenomena typical of biological materials. a) – b) First the material is removed uniformly across the whole area. c) after about 720 sec. small holes, so called sputter spots, form and grow, while the interior of the box is milled uniformly into the material.

Also the angle of incidence of the ion-beam on the sample has an effect on the sputter process (Xu *et al.*, 1992; Vasile *et al.*, 1999). This was tested on a bamboo fibre cell wall, which is a highly oriented cellulose fibre composite. Boxes of 3.0 µm × 3.0 µm × 1.0 µm in size were milled perpendicular to the long fibre cell axis at different ion beam currents (70 pA, 150 pA, 350 pA, 1000 pA and 2700 pA) and at different angles (0°, 10°, 25° and 45°) using a dwell time of 1.0 µs and an overlap of 50 %. The milled boxes are shown in Figure 1.12 a). In Figure 1.12 b), the beam currents and the angles of incidence are given for each box:

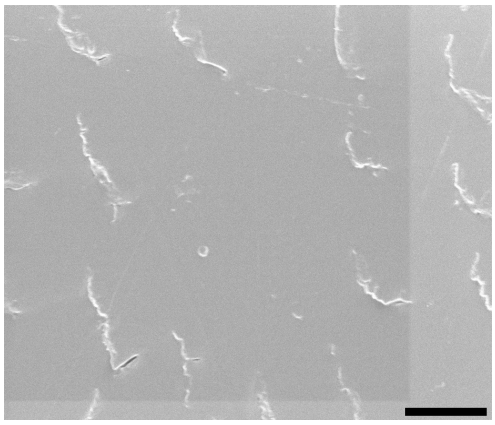

a) First picture of the milling area, t = 0 s.

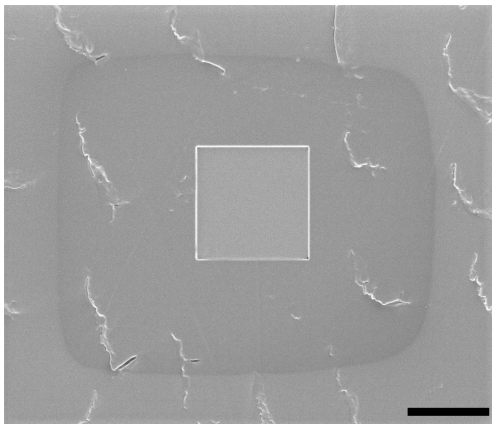

b) Early stage of the milling process t = 240 s.

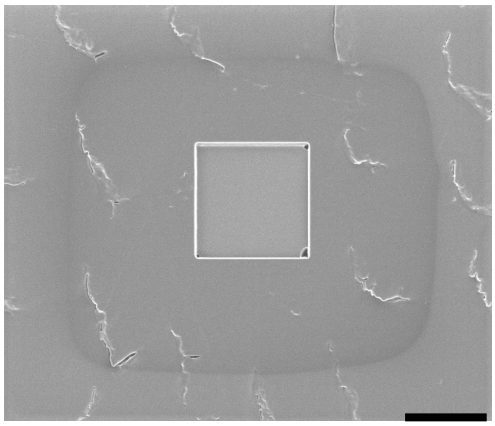

c) Two sputter spot have been developed, t = 720 s.

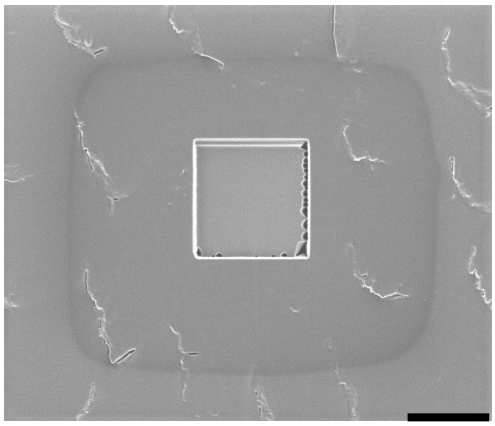

d) Formation of several sputter spots at the right edge of the box, t = 960 s.

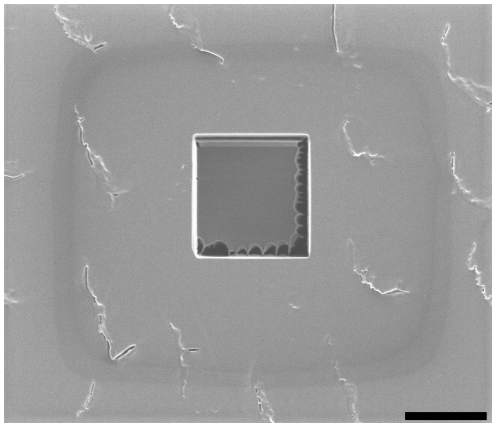

e) Growing of the sputter spots, t =1440 s.

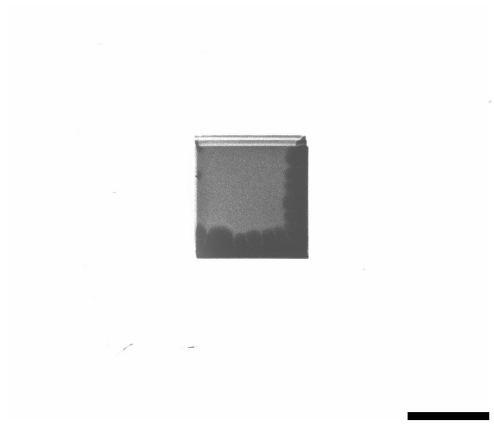

f) Last micrograph of the sputter process, t = 1920 s.

Figure 1.11: Progress in milling, the length of the black bars is 5 µm (FIB micrographs; milling parameters: beam current = 70 pA, dwell time= 1.0 µs and overlap = 50 %).

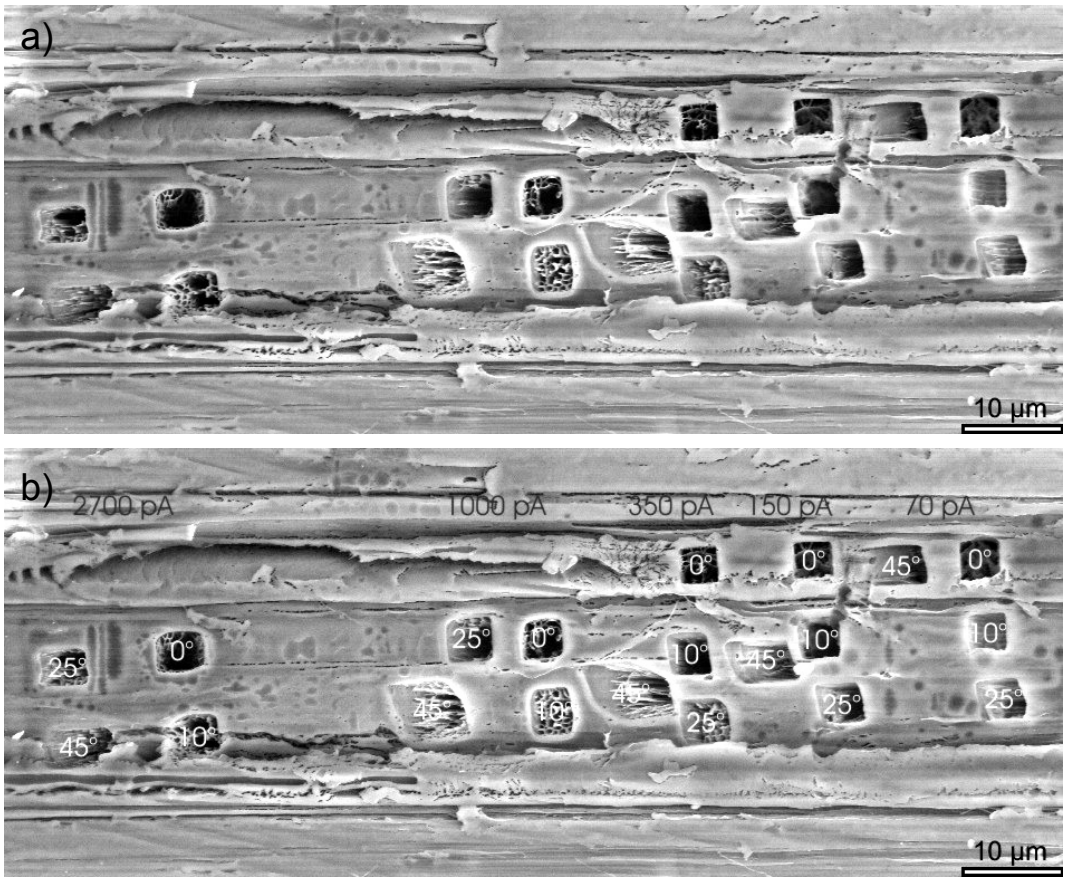

Figure 1.12: a) SEM micrograph of the bamboo specimen, the fibre cell is oriented horizontally, b) Ion beam currents and angles of incidence (SEM micrographs).

In some of the boxes, material remains which was not sputtered away. The remaining material forms a pillar or a net-like structure. With increasing beam current and increasing angle, the amount of remaining material increases.

1.5.2 Sputter rates

During the milling experiments, it became apparent that the sputter rates, i.e. the volume of material sputtered away per beam current and time (in $\mu m^3/nAs$), are higher for biological materials than for technical materials, such as silicon, copper, aluminium, etc. (see Table 1.2 – 1.4). In the following section, experiments are described with which the sputter rate for insect cuticle was determined.

To determine the sputter rate of insect cuticle, two specimens were investigated: (i) a piece of the upper wing (elytron) of the mealworm beetle of the species *Tenebrio molitor* and (ii) the upper leg of beetle *Pachnoda marginata*. On the wing boxes of $3.0\ \mu m \times 3.0\ \mu m \times 0.5\ \mu m$ and on the leg boxes of $4.0\ \mu m \times 4.0\ \mu m \times 1.0\ \mu m$ were milled for different values of dwell time and overlap.

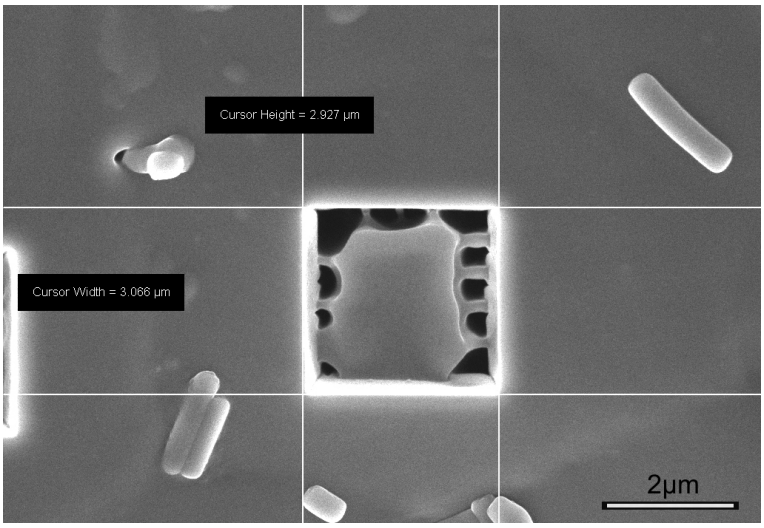

Figure 1.13: Measurement of the x and y component of the milled box No.21
on the upper wing (elytron) of a mealworm beetle (*Tenebrio molitor*) (SEM micrograph).

The resulting x and y dimensions of the milled boxes were measured in the SEM (Figure 1.13). The z value for each box was determined with a white light interferometer. The results are visualised in different ways: The 3-D plot (Figure 1.14) reveals the profile of the box, this illustrates the roughness of the bottom surface of the box. The surface line-scan describes the topography of the box and can be used to measure the depth of the box. The z value was measured between the lower top edge of the milled box and the mean level of the bottom (Figure 1.15).

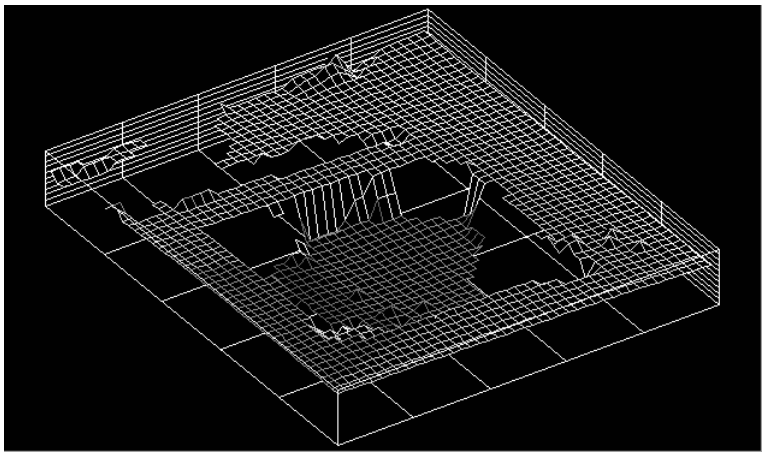

Figure 1.14: White light interferometer 3-D plot of sample (i) box No. 21
(White light interferometer image).

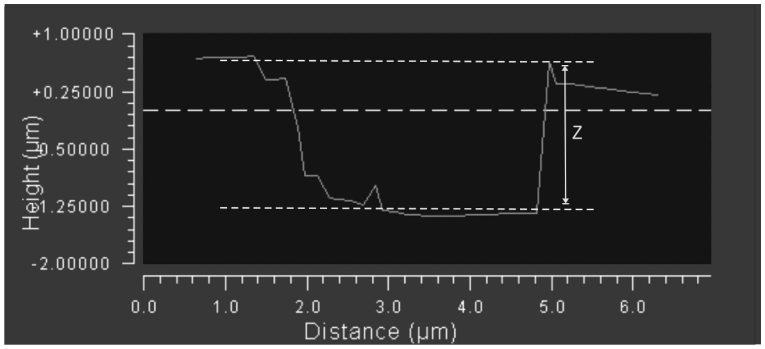

Figure 1.15: White light interferometer depth profile of sample (i) box No. 21
(White light interferometer image).

Sputter rates were calculated from the measured values. The measured x, y and z values and the calculated sputter rates for the two insect cuticles are listed in Tables 1.2 and Table 1.3. For comparison, sputter rates for Cu, Si and Al are given in Table 1.4 from the FIB manufacturer's manual (fei, 1996).

Table 1.2: Milling parameters, box dimensions (x, y, z) and sputter rates for the elytron of the beetle *Tenebrio molitor*. The ion beam current was constant at 0.15 nA and the milling time was held constant at 202 s for a box sized 3.0 µm × 3.0 µm × 0.5 µm.

Box No. on sample (i)	Dwell time [µs]	Overlap [%]	X [µm]	Y [µm]	Z [µm]	Sputter rate [µm³/nAs]
1	1.0	50	3.05	2.97	2.11	0.632
2	1.2	50	3.02	3.03	1.50	0.454
3	1.4	50	3.03	3.03	1.55	0.469
4	1.4	50	3.10	3.06	1.72	0.539
5	1.6	50	3.07	3.05	1.92	0.593
6	1.8	50	3.10	3.08	1.78	0.562
7	2.0	50	3.10	3.07	1.88	0.588
8	2.2	50	3.10	3.03	1.92	0.595
9	2.2	50	3.09	2.98	1.45	0.439
10	2.4	50	3.05	3.05	1.52	0.467
11	2.6	50	3.06	3.05	1.45	0.448
12	1.0	50	3.10	2.97	1.50	0.455
13	1.0	60	3.09	3.03	1.55	0.477
14	1.0	70	3.11	3.05	1.64	0.514
15	1.0	80	3.08	3.03	1.29	0.397
16	1.0	90	3.04	3.03	1.55	0.470
17	1.0	100	3.06	3.06	1.83	0.566
18	1.2	60	3.10	3.00	1.83	0.561
19	1.4	70	3.07	3.00	1.83	0.556
20	1.6	80	3.09	2.99	1.50	0.458
21	1.8	90	3.07	2.93	1.69	0.500
22	2.0	100	3.07	2.99	1.88	0.569

Table 1.3: Milling parameters, box dimensions (x, y, z) and sputter rates for the beetle leg *Pachnoda marginata*. The ion beam current was constant at 0.148 nA and the milling time was held constant at 300 s for a box sized 4.0 µm × 4.0 µm × 1.0 µm.

Box No. on sample (ii)	Dwell time [µs]	Overlap [%]	X [µm]	Y [µm]	Z [µm]	Sputter rate [µm³/nAs]
23	1.6	80	4.06	4.06	1.48	0.547
24	1.6	80	4.11	4.14	1.90	0.728
25	1.8	90	4.14	4.13	1.37	0.528
26	1.8	90	4.00	4.03	1.68	0.611
27	1.4	70	4.06	4.04	1.65	0.608
28	1.4	70	3.99	4.05	1.74	0.632

Table 1.4: Sputter rates for technical materials (fei, 1996).

Material	Dwell time [µs]	Overlap [%]	Sputter rate [µm³/nAs]
Copper	1.0	50	0.375
Aluminium	1.0	50	0.500
Silicon	1.0	50	0.150

The values for the sputter rates measured for insect cuticle (Table 1.2 and 1.3) show no direct correlation to the dwell time and the overlap. However, the values obtained for the Tables 1.2 and 1.3 are higher than those of most of the technical materials shown in Table 1.4. Only a small range of dwell time and overlap was used in the experiments, further investigations with a wider range of these values will be carried out in the future.

1.6 Influence of the Ga^+-ion beam on the sample material

After a closer inspection of the features created during milling on bamboo and insects cuticle, the question arose whether the resultant topography is a structural feature of the material or an artefact of the interaction of the ion beam with a hierarchically structured composite material. The influence of the 30 keV Ga^+-ion beam was investigated in detail, qualitatively and quantitatively, in order to estimate, which artefacts occur, how large the affected volume is, by how much the samples temperature rises, and by how much the mechanical properties change.

1.6.1 Redeposition

Redeposition of sputtered material is one of the known major problems during milling. An example for this is shown in Figure 1.16 a): a cut in a hair of a housefly. After milling, the specimen was tilted by 45° and a micrograph was taken showing a side view of the specimen. Figure 1.16 b) shows the cut into the hair and the redeposited gallium and cuticle material, which forms large conglomerates sticking to the hair.

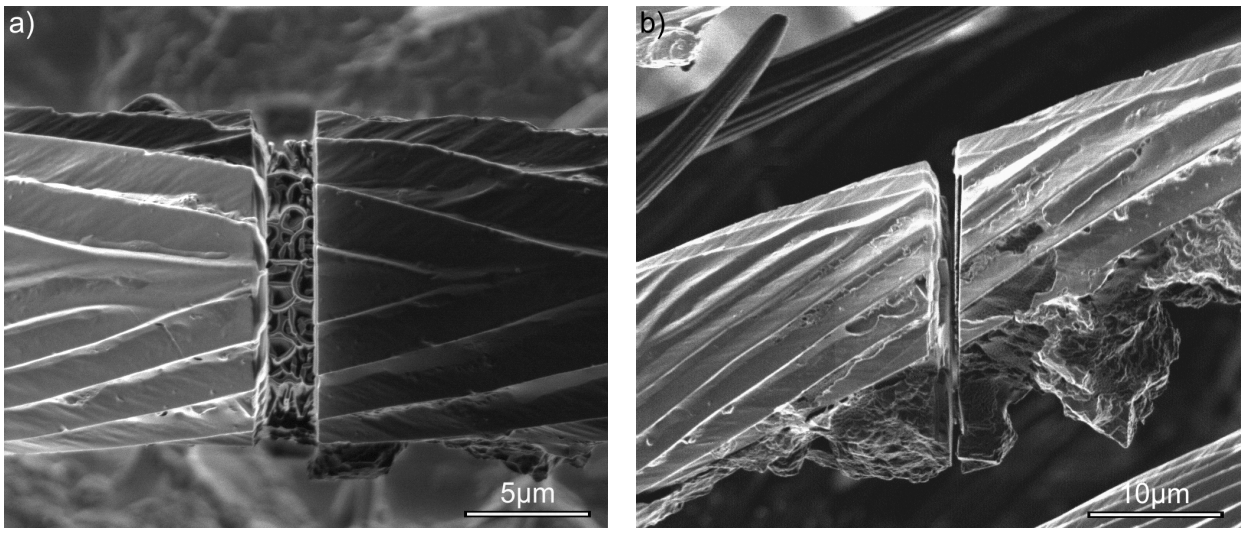

Figure 1.16: a) Top view of a box milled into the hair of a housefly (*Musca domestica*).
b) Sample tilted by 45° showing redeposition after milling (FIB micrographs).

1.6.2 Ga^+-ion implantation

The interactions of Ga^+-ions with the target material are very complex. Some of the incoming Ga^+-ions recoil at the targets surface, others are implanted into the sample surface. A first qualitative measurement of the ion implantation was to examine one of the milled boxes of the beetle wing *Tenebrio molitor*, Sample (i) in the SEM Leo 1530 VP. The SEM is equipped with an Energy-Dispersive X-ray analysis system (EDX) to map the distribution of the different chemical elements. The elemental distributions of carbon, oxygen and gallium obtained by EDX are shown in Figure 1.17.

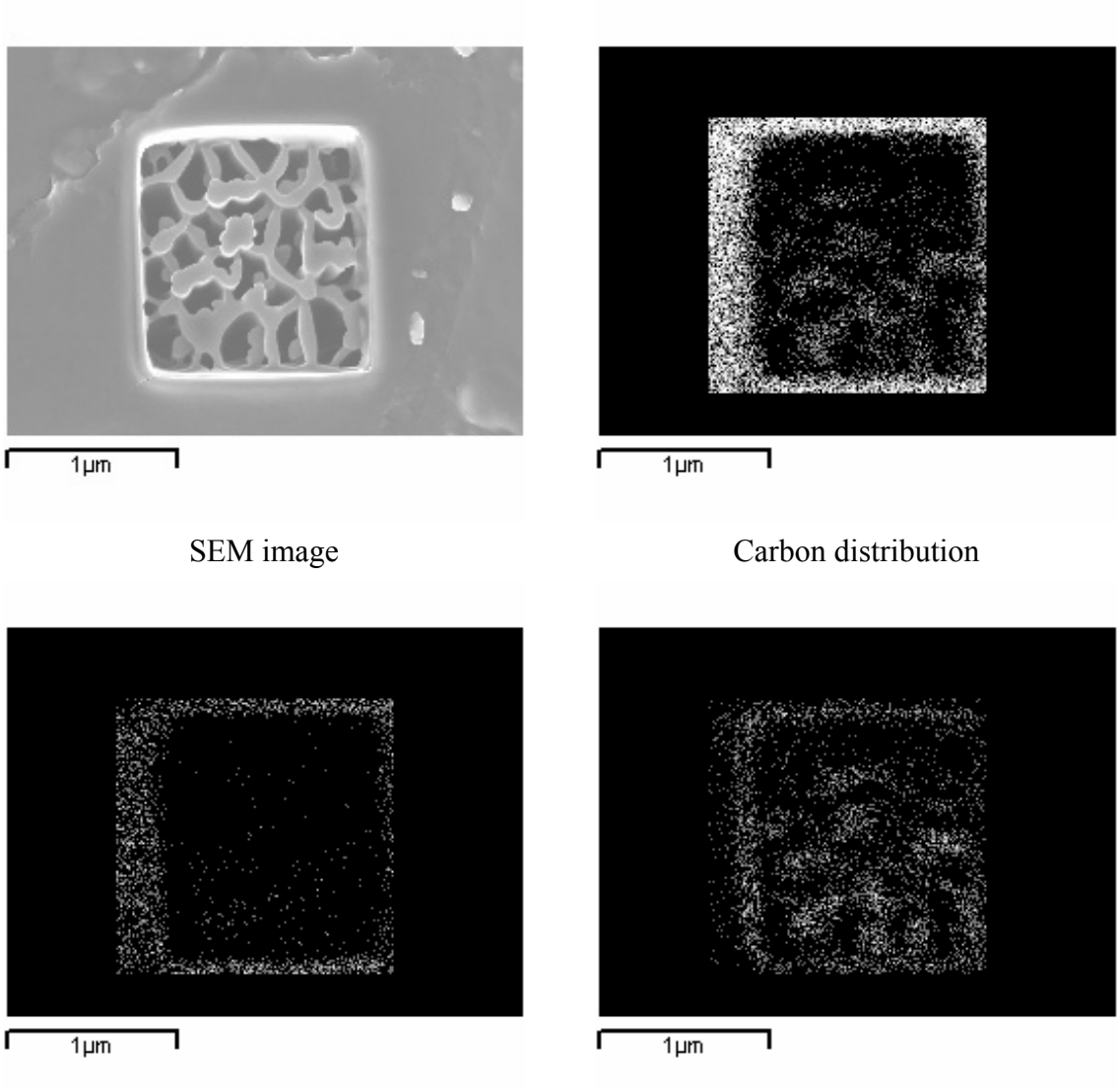

Figure 1.17: SEM overview and elemental distribution maps of C, O and Ga.

The gallium distribution map confirms the presence of significant amounts of gallium in the milled area.

1.6.3 Temperature rise due to the ion bombardment

Another consequence of the ion bombardment is a rise in sample temperature. This can influence the material properties in different ways. A moderate heating of the sample by about 50 K will lead to a loss of moisture in the sample, a larger rise in temperature can lead to structural changes, such as crystalline-amorphous transitions, break-up of chemical bonds, the denaturation and decomposition of the material, or melting.

The heating under the influence of a uniform ion beam incident on a semi-infinite solid has been calculated by two studies to date (Melngailis, 1987; Ishitani and Kaga, 1995). Melngailis (1987) equates the thermal energy current flowing out of a hemisphere of radius ρ into a semi-infinite solid to the input power, neglecting radiative (or other) heat losses from the samples surface. He calculates the resultant temperature rise ΔT_1 to be:

$$\Delta T_1 = \left(\frac{V \cdot J}{2\kappa}\right) \cdot \left(\frac{r^2}{\rho}\right) \qquad [1.1]$$

where V is the ion acceleration voltage, J the current density (beam current divided by the beam diameter), κ the thermal conductivity, r the beam radius and ρ the radius of the affected volume. This equation holds for $\rho \geq r$. Setting $\rho = r$ and with $d = 2r$, the maximum ΔT_1 at the circumference of the ion beam can be calculated:

$$\Delta T_1 = \left(\frac{V}{\kappa}\right) \cdot \left(\frac{I}{d}\right) \cdot \left(\frac{1}{\pi}\right) \qquad [1.2]$$

where, I is the beam current and d the spot size. Ishitani and Kaga (1995) calculated the rise in temperature assuming a Gaussian type power profile, neglecting all losses via sputtering, lattice damage, electron emission and ion backscattering. They calculated the rise in temperature ΔT_2 to be:

$$\Delta T_2 = \left(\frac{V}{\kappa}\right) \cdot \left(\frac{I}{d}\right) \cdot \left(\frac{1}{\pi^{1/2}}\right) \qquad [1.3]$$

For semi-bulk material, the rise in temperature ΔT_2 increases by a factor of 2, and for sheet samples and pillars to a factor of just under 4.

The temperature rise calculated according to the model of Melngailis (1987) is lower by a factor of $\pi^{1/2} = 1.77$ than that calculated according to Ishitani and Kaga (1995).

The thermal conductivities of only few biological materials are known. Assuming the thermal conductivity of insect cuticle to be similar to wood-cell wall material (0.44 - 0.88 W/mK; Dinwoodie, 2000), another polysaccharide fibre composite, the temperature rise was calculated. As a reference the temperature rise of the polyimide Kapton® was calculated. The values of the thermal conductivity of Kapton® were obtained from data sheets (Goodfellow, 2005). The diameter of the beam at different beam currents was obtained from the manual of the FIB system used (fei, 1996). The rise in temperature was calculated for bulk material using Equations [1.2] (Table 1.5) and [1.3] (Table 1.6). For cutting samples in the µm-range and for tungsten deposition using the GAD system, typical ion beam currents of 70 pA and 150 pA were used respectively, their values are marked in Tables 1.5 and 1.6.

Table 1.5: The rise in temperature ΔT_1 calculated using Equation [1.2] (Melngailis, 1987) for bulk material $r = \rho$, $V = 30$ kV.

I [nA]	d [µm]	Polyimide (Kapton®)		Wood	
		$\kappa = 0.10$ W/mK	$\kappa = 0.35$ W/mK	$\kappa = 0.44$ W/mK	$\kappa = 0.88$ W/mK
		ΔT_1 [K]			
0.001	0.008	11.9	3.4	2.7	1.4
0.004	0.012	31.8	9.1	7.2	3.6
0.011	0.015	70.0	20.0	15.9	8.0
0.070	0.025	267.4	76.4	60.8	30.4
0.150	0.035	409.3	116.9	93.0	46.5
0.350	0.055	607.7	173.6	138.1	69.1
1.000	0.080	1193.7	341.0	271.3	135.6
2.700	0.120	2148.6	613.9	488.3	244.2

Table 1.6: Rise in temperature ΔT_2 calculated using Equation [1.3] (Ishitani and Kaga, 1995) for bulk material, $V = 30$ kV.

I [nA]	d [µm]	Polyimide (Kapton®)		Wood	
		$\kappa = 0.10$ W/mK	$\kappa = 0.35$ W/mK	$\kappa = 0.44$ W/mK	$\kappa = 0.88$ W/mK
		ΔT_2 [K]			
0.001	0.008	21.2	6.0	4.8	2.4
0.004	0.012	56.4	16.1	12.8	6.4
0.011	0.015	124.1	35.5	28.2	14.1
0.070	0.025	473.9	135.4	107.7	53.9
0.150	0.035	725.4	207.3	164.9	82.4
0.350	0.055	1077.1	307.7	244.8	122.4
1.000	0.080	2115.7	604.5	480.8	240.4
2.700	0.120	3808.3	1088.1	865.5	432.8

The expected rise in temperature due to the ion bombardment is thus significant.

1.6.4 Change in mechanical properties

The incorporation of Ga^+-ions and the temperature rise in the material due to the ion bombardment are expected to alter the mechanical properties of the exposed sample material. To study the extent of this effect, experiments were performed with the polyimide Kapton® as reference material. A 125 µm thick Kapton® foil was exposed to different amounts of ions (described by the fluence, the beam current times exposure time divided by the elementary charge and the exposed area [ions/cm²]) in the FIB. After exposure to the ion beam, the hardness and the Young's modulus were measured using an MTS Nanoindenter SA2 system. This nanoindenting system can operate in a mode which allows a depth-dependent investigation of the material by continuous oscillation of the indenter tip during the penetration (Harmonic Contact Stiffness Method). Several indents were made in exposed and in unexposed areas. Figure 1.18 shows a plot of hardness versus fluence for different penetration depths. Each data point is the mean value of 5 to 9 indents. The data point at zero fluence represents the unexposed material. The hardness versus the fluence is plotted in a uniform greyscale for given indentation depths.

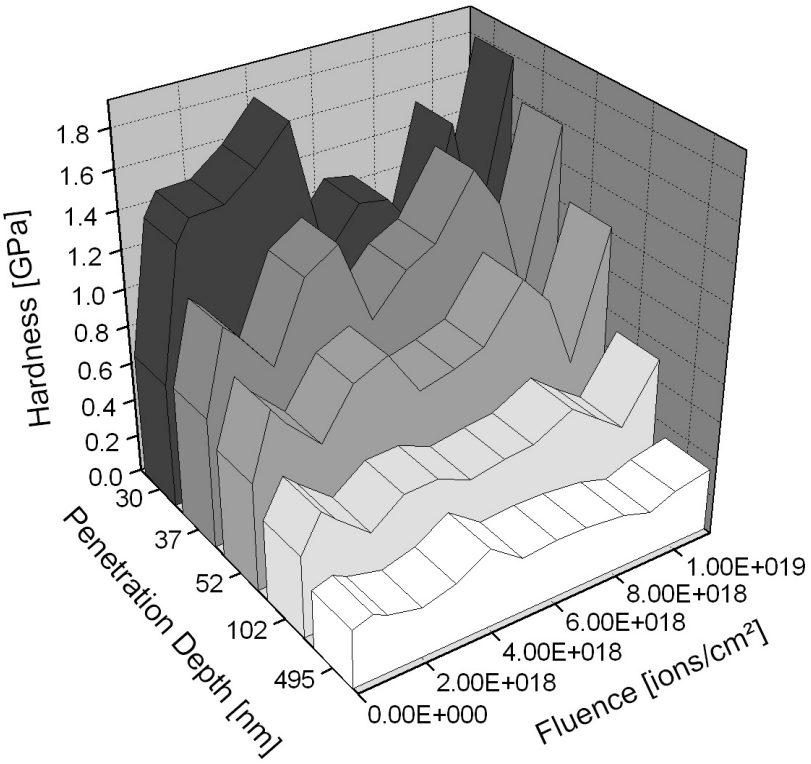

Figure 1.18: Hardness plotted versus fluence, measured for different depths.

In Figures 1.18 and 1.19 the measured values for the hardness and Young's modulus at zero fluence (which is the unexposed material) decrease with increasing indentation depth. This is

an artefact caused by the nanoindentation technique. The hardness measured close to the surface up to 52 nm show that the influence of the ion beam on the sample material was significant. Below that depth, the material properties quickly approached those of the unexposed material. A similar trend was observed in Figure 1.19, where the measured Young's modulus is plotted against the fluence for the same penetration depths.

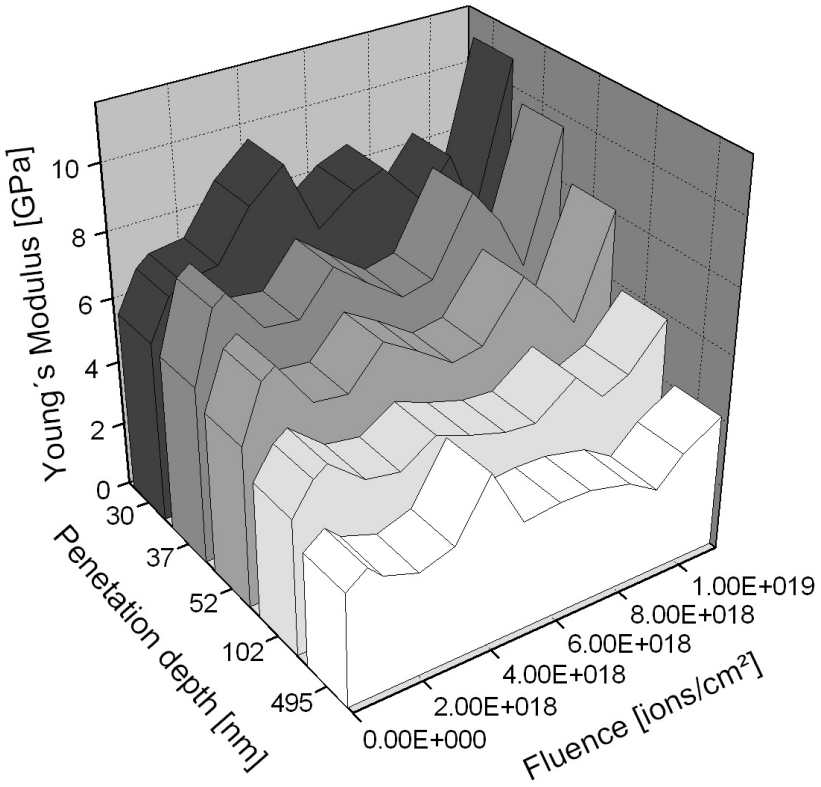

Figure 1.19: Young's modulus versus the fluence, measured for different depths.

Again the influence on the Young's modulus is significant for indentation depths up to a depth of 52 nm. However, deeper in the polyimide sample material the material properties are almost unaffected by the bombardment of the Ga^+-ions.

1.7 Discussion

The experiments and results described above show that the FIB is a powerful tool for the investigation of the two- and three-dimensional structure of biological materials. As other techniques, it has advantages and disadvantages.

FIB microscopy and milling

The FIB system can be used as an SEM for high resolution microscopy. Especially for biological materials, the FIB system caused, during imaging, fewer charging effects on non-conductive specimens than the SEM. This is presumably because the gallium, which is accelerated onto the sample surface, builds up a thin conductive layer over which charges can be spread and therefore reduced. However, the Ga^+-ion beam damages the sample surface even during imaging. Thus even if the system is used for imaging, low beam currents should be used in order to limit the beam induced damage. The adjustment of the focus is preferably carried out at a position outside the region of interest.

A thin conductive layer can be deposited onto the sample before imaging. The conductive layer (gold/palladium or carbon) has some advantages: it reduces charging effects which are caused by the Ga^+-ions and at the same time it can be used as a protective layer to reduce ion beam damage.

The experiments on a wide range of biological materials (chitin, keratin and cellulose composites) described above showed that all can be milled with great precision. Generally it was found that a lower beam current leads to smoother cutting edges. This is for two reasons: first, the intensity of the beam is non-uniform, it has a Gaussian distribution with a maximum in the centre. Second, an increasing beam current enlarges the beam size and with it the spot size. The diameter of the beam at different beam currents is listed in Table 1.5. For beam currents higher than 70 pA (used for biological materials) the ion beam does not exhibit a well defined spot with a diameter of 0.025 µm but damages the material around the defined milling area significantly. Ishitani *et al.* (1995) found ion beam damage, the so called sputter spots which are small holes in the material, 50-100 nm away from the dug area.

Structural investigations

The power of the FIB system for the investigation of complex structures was demonstrated on the hairy attachment system of the beetle *Gastrophysa viridula* and the filiform sensors found on the cerci on crickets *Acheta domesticus*.

The investigation of the performance and arrangement of the hairy attachment system of the beetle *Gastrophysa viridula* (Figure 1.4) was possible because the FIB system allows site specific milling, which induces no mechanical influence on the sample. Without embedding, no other cutting technique allows to cut the setae in contact with the surface, without destroying the setae or breaking the contact. By tilting and rotating the sample stage, the geometry of every individual seta, the distance to their next neighbours, the number of setae in contact, the pattern and the arrangement of the setae can be investigated. Such information is required for a better understanding of the attachment systems and its performance in insects and its emulation in man-made materials and structures.

The cross-section of the filiform sensor of Figure 1.7 shows its shape in three dimensions and a detail not seen in optical micrographs of microtome sections in two dimensions and TEM. (Figure 1.8; Seidel, 2005; Gnatzy *et al.*, 1971; Keil, 1998). In contrast to the FIB, standard biological sample preparation techniques, such as embedding and microtome sectioning, cause artefacts in the samples such as cracks in brittle materials, for example. Another benefit of the FIB system is that the samples can be prepared site specifically. Due to the high magnification and accuracy of the system, cross-sections can be cut of the features of interest. Cross-sections made with a microtome are not site specific, because the orientation of cutting an embedded sample cannot be controlled as well as in the FIB.

Structural features and milling artefacts

During the milling of biological samples, the formation of a net-like or pillar structure was frequently observed (Figures 1.12 and 1.16 a). This raises the question whether these structures are features or artefacts caused by the ion-beam. Ishitani *et al.* (1995) described the same phenomena during milling of a housefly's eye and human hair. However they do not explain the cause for the spots and the net structure. There are a number of possible reasons for the development of such a rough structure after milling.

One reason may be that the milling-rate is not constant over the area. Figure 1.11 shows the formation of sputter spots at the right side during milling of a box in the insect cuticle. These sputter spots enlarge and new ones appear in their vicinity during further milling. The material in between is reduced, leading to a structure with a net-like appearance. This structure changes into a pillar structure on further milling.

The surface of biological materials is often structured and rough, natural plane surfaces are very rare. By milling through a structured surface the sputter rate varies over the milling area since the angle of incidence varies. As the angle between the incident ion and the sample surface is decreased (from 90° to 0°), the yield, which is the number of sample atoms removed per incident ion, for physical sputtering goes through a maximum, between 70° to 80° (Stark *et al.*, 1996; Vasile *et al.,* 1999). This leads to non-uniform milling of the surface and causes artefacts.

Experience shows that there is no correlation between the atomic weight or density of different materials and the sputter rates. Table 1.4 illustrates this: for the same dwell time and overlap, 1.0 µs and 50 % respectively, copper (atomic weight 63.55), has a sputter rate of 0.375 µm³/nAs (fei manual) which is only 75 % the sputter rate of aluminium (atomic weight 26.98) with a sputter rate of 0.500 µm³/nAs (fei manual).

Young *et al.* (1993) describe that during the FIB milling of mites the ion beam can easily mill through the cuticle, but not with a constant milling rate and that the ion beam preferentially mills “softer” material. He also states that the “harder” material remains as a pillar or net structure. From a material science point of view, it is not clear, however, what Young *et al.* mean by “harder” and “softer” materials. Since the sputter rate is the result of elastic and inelastic collisions of the high accelerated Ga^+-ions with the atoms and ions on the sample surface, the impact energy of the ions must be higher than the binding energy of the elements and molecules of the sample, in order to break bonds and remove material. Thus, the weaker the binding energy is, the more of the sample surface can be sputtered. This is reflected by the fact, that metals with relatively weak binding energies have a higher sputter rate (sputter rate Cu: 0.375 µm³/nAs; Al: 0.500 µm³/nAs, dwell time: 1 µs, overlap: 50%; fei manual) than ceramics with stronger ionic or covalent bonds (sputter rate Si: 0.150 µm³/nAs, dwell time: 1 µs, overlap: 50%; fei manual).

The 125 µm thick polyimide (Kapton®) foil, which was exposed to different fluences, for the investigation of the change in the mechanical properties due to the ion beam, showed some circular holes in the exposed area. He *et al.* (1998) describe similar craters after the exposure of Kapton® with Ar^+, N^+, He^+ and D^+ ions. They suggest that hillocks are formed by the creation of blisters created by gas pressure. Gases which are formed during the ion bombardment diffuse through the material until they are trapped in defects and start to build cavities. These blisters can break, the trapped gases are released and this leads to the holes found on Kapton® after the exposure to the ions. However, the formation of hillocks was not observed in the exposed areas of the Kapton® foils during the experiments for this thesis.

The irregular structure of the milling area may also be due to shrinkage of the material. The combination of the vacuum of the specimen chamber and high energy impact causes a loss in moisture content of the sample, leading to sample shrinkage. Aubry *et al.* (2002) observe a shrinkage of the sample while etching polymers (PMMA, polyimide) with the FIB. The shrinkage of polymers in the FIB is possible due to the outgasing of short chained or unsaturated components of the polymer and coiling up of the polymer chains under the influence of the beam.

Sputter rates

The sputter rates for a number of technical materials are known. Sputter rates measured on insect cuticle (Table 1.2 and Table 1.3) using the same dwell time and overlap as for the technical materials (1 µs and 50%, respectively), range from 0.455 to 0.632 μm^3/nAs. This reveals that the sputter rate of this biological material is comparable to that of aluminium (0.500 μm^3/nAs).

However, in the results listed in the Tables 1.2 and 1.3 no clear dependence of the sputter rates on dwell time and overlap for insect cuticle can be seen. Further investigations are necessary, with larger variations in these parameters in order to gain the best settings for the milling of biological materials, expressed by the sputter rates. Overall, milling large volumes in biological materials is still time consuming. The milling time may be reduced by the use of a GAE system. Especially the selective carbon milling accelerates the milling procedure for polymers and biological samples. However, lacking the availability of this piece of equipment, its efficiency could not been tested on biological materials during the preparation of this thesis.

Influence of the Ga^+-ion beam

Redeposition

One major problem during the milling of polymeric and biological (and other) samples is the redeposition of a mixture of sputtered material and gallium in the milling and the surrounding area. In Figure 1.16 b) large amounts of material were redeposited, making the sectioning of the sample difficult and even impossible. This phenomenon is of importance also when structures are milled into bulk materials. Fu *et al.* (2000) reported this, too, illustrating that the milling of structures with a high aspect ration (>1) is problematic, because the sputtered material precipitates at the inside walls of the structure.

There are procedures to avoid or minimise redeposition. One way is to use low beam currents and small spot sizes for milling. Another is to mill stepwise into the bulk material. Young *et al.* (1993) milled boxes with different sizes getting smaller one after another in order to get a better aspect ratio for the milling of large volumes. Both strategies worked well in the experiments performed for this thesis. Milling one box after another with increasing depth, instead of a larger single box, reduces the milled volume at a given time and with it the amount of redeposited material. Finally, milling with a low beam current (<70 pA) along a small box or line at the cutting edge, leads to a "clean" cross-sections with hardly any redeposition.

If the sample is a free standing structure, redeposition is less of a problem than during milling in bulk materials. Most of the milling during this thesis was performed in order to prepare cross-sections of free standing structures. For those, the fine cleaning mode of the FIB system was used with low beam currents (~ 70 pA). In this mode the beam mills along a line and the line propagates towards the sample, in other words, a line was milled one after another. Using this technique, sharp cross-sections were obtained, showing no redeposition.

Some other techniques can be found in the literature in order to prevent redeposition: tilting the sample before milling is started reduces the amount of redeposited material (Fu *et al.*, 2000). A similar effect is achieved with a two stage procedure, in which a narrow wall of material is left to act as a shield to redeposition, while the balk of the material is removed (Yongqi *et al.*, 2000).

For milling holes with large aspect ratios in the bulk material, gas assisted etching (GAE) can be used. Using it, the sample material is rather chemically etched than physically sputtered in order to reduce redeposition on the sidewalls or surrounding structures.

Ga^+-ion implantation and stopping range of the Ga^+-ions

Using EDX measurements, gallium was found in significant quantities in the milled area. Such EDX investigations cannot, however, reveal whether the detected gallium covers the surface of the milled area, or if it is implanted into the sample. A knowledge of the implantation depth of the ions is necessary in order to estimate the volume fraction of the sample material, which is influenced by the ion beam in its structural and mechanical properties.

For the estimation of the stopping range of the 30 keV Ga^+-ions, a Monte-Carlo simulation was used (Appendix 6.1). Ziegler and Biersack (2004) developed the Monte-Carlo simulation tool TRIM, which allows the calculation of the stopping range of ions in solids. For a simulation, several parameters of the sample material are required such as the elements of the sample material, the binding energies and the binding conditions (distance to the next neighbours, binding angles, geometries, etc). For biological materials, these parameters are not known, so a reference material of known and uniform material properties, the Polyimide Kapton®, was chosen.

The newest version of TRIM in SRIM 2003.26 was used to calculate the stopping range of 1000 ions which are accelerated with an energy of 30 keV towards a 125 µm thick polyimide (Kapton®) foil. The material parameters for Kapton® were found in the material library of the program TRIM. The minimum, mean and maximum stopping ranges and the radial distances from the incident position (lateral x: 0, y: 0) of the stopped ions are listed in Table 1.7. The frequency, lateral and volume distributions can be found in Appendix 6.1.

Table 1.7: Simulated minimum, mean and maximum stopping range and radial distribution of the 30 keV Ga^+-ions in a 125 µm thick polyimide (Kapton®) foil using the Monte Carlo simulation TRIM (Ziegler and Biersack, 2004).

	Minimum [nm]	Mean [nm]	Maximum [nm]
Stopping range	13.6	36	73
Radial distribution	0.2	8.6	30

From the TRIM simulation one can assume for Kapton® that a 36 nm to 73 nm thick surface layer is influenced by the gallium ions. The bulk material in a depth beyond 73 nm (maximum stopping range of the ions) should, according to the simulation, not be affected by the implantation of the ions.

Temperature rise in the sample

The temperature rise in the bulk material due to the ion beam was calculated using the equations derived by Melngailis (1986) and Ishitani and Kaga (1995) (Tables 1.5 and 1.6). In biological materials, a rise of 10 to 50 K will lead to a loss in moisture content (the remaining bonded water of the sample) and result in a change in their mechanical properties, a shrinkage of the sample and/or the formation of cracks due to drying-effects, depending on the amount of water loss. A higher temperature can lead to transformations from ductile to brittle (above the glass transition temperature T_g in polymeric materials, typically 200-300°C). Also phase transitions from crystalline to amorphous or vice versa may occur, depending on the type of material. At higher temperatures, the material will begin to melt or to decompose.

A Kapton® foil (Type 100 HN, 25 µm thick) contracts on its first exposure to elevated temperatures due to the manufacturing process. It will contract by 0.17 % when it is exposed to 150°C for 30 min, and by 1.25% when it is exposed to 400°C for 120 min. Between 360°C and 410°C the glass transition temperature T_g is reached and the polymer changes its mechanical properties from glassy to viscoelastic. Kapton® starts to decompose at ~ 460°C and the temperature of 10% weight loss is ~ 540°C (heating rate 3°C/min) (DuPont data sheets, 1997).

Even for low beam currents the residual ΔT will lead to the contraction of a Kapton® foil during sample preparation. However, the contraction is caused by the manufacturing process

of the Kapton® foil and will only occur during the first heating cycle of the sample. Afterwards the sample should be stable. A beam current of 70 pA will lead to a temperature rise ΔT_2 of 473.9 K in the Kapton® sample, according to Equation [1.3] (Ishitani and Kaga, 1995; $\kappa = 0.10$ W/mK, Goodfellow)). Even for this relatively low beam current the rise in temperature is sufficient to reach the regime, where Kapton® starts to decompose. For cutting samples from a Kapton® foil a beam currents up to 1000 pA were used, which led to a calculated ΔT_1 = 1194 K and ΔT_2 = 2116 K ($\kappa = 0.10$ W/mK, Goodfellow). The Kapton® material is therefore expected to decompose rapidly and the milling process can be estimated to be a combination of physical sputtering and thermal decomposition. This may also provide another explanation for the structural features observed during the milling process.

The question remains, which temperature rise is harmful for biological materials. Kim *et al.* (1994) investigated the thermal characteristics of chitin. Using a dynamic mechanical analysis and differential scanning calorimetry (heating rate 5°C/min), they could show that chitin has a glass transition at 236 °C due to the relaxation of the polymer main chain. Polysaccharides, like chitin and cellulose, decompose before they reach their melting temperature. Kim *et al.* (1994) showed that chitin starts to decompose at 250 °C. The temperature of 10% weight loss was found to be 287 °C (heating rate 5°C/min). A temperature rise of less than 200 K due to the ion bombardment is still not harmful to the chitin fibres of the insect cuticle, but may influence the surrounding protein matrix.

An important parameter for the calculation of ΔT is the thermal conductivity of the specimen. According to Equations [1.2] (Melngailis, 1986) and [1.3] (Ishitani and Kaga, 1995), low values of the thermal conductivity for biological materials and Kapton® lead to a significant rise in temperature during the exposure to the ion beam. However, due to the low value, the affected volume is very small and nearly thermally isolated.

Change in mechanical properties

The influence of the ion beam bombardment on the mechanical properties of the samples was investigated by measuring the mechanical properties of a 125 µm thick Kapton® foil exposed with different fluences (ions/cm²) in the FIB (Chapter 1.6.4). Figures 1.18 and 1.19 show a significant influence of the fluence on the mechanical behaviour of the Kapton® in depths close to the surface (30 to 52 nm), but in penetration depths beyond ~ 100 nm, the change in the mechanical properties is not so obvious.

From the results of the simulated stopping range of the ions using the Monte-Carlo simulation TRIM (Ziegler and Biersack, 2003) one would expect that the mechanical properties of the material change within a 36 to 73 nm thick surface layer, which is in the range between the mean and the maximum simulated stopping range. If the simulation according TRIM is correct, then there should be no significant influence of the ion beam on the mechanical properties beyond a depth of 73 nm. This is consistent with the measured changes in mechanical properties using the nanoindentation technique. The mechanical properties change within a surface layer of ~ 100 nm, beyond this mark there is no change due to the ions, simply because the gallium ions cannot penetrate to larger depth.

For a constant penetration depth, the influence of the ion beam fluence on the mechanical properties of the sample material can be investigated. At 30 nm, for example, a relative increase in the Young's modulus of 22% from 5.84±0.31 GPa (fluence: 0 ions/cm², unexposed material) to 7.13±0.76 GPa (fluence: 1.01×10^{18} ions/cm²) can be found at first. It levels off with increasing fluence. The values start to fluctuate (increase and decrease), but they stay always above the values of the unexposed sample material. There is no significant trend visible in the change of the mechanical properties dependent on the fluence.

The ion bombardment leads not only to an implantation of the ions, but also to a sputtering of the sample surface. For higher fluences, the volume in which the ions are implanted will be sputtered in a scanning cycle and at the same time the newly formed surface will be influenced by the ion beam. For higher fluences a steady state would be expected in which the volume fraction, which is affected by the implantation, shows constant mechanical properties. But for the fluences tested this is not the case, as Figures 1.18 and 1.19 reveal.

For the exposure of the Kapton® samples relatively high ion beam currents (up to 2700 pA) were used in order to achieve high fluences. The Kapton® material is thought to decompose during the exposure with the ions because the rise in the local temperature is significant, as described above. So the mechanical properties measured close to the samples surface are expected to differ from those of the unexposed material.

Ion implantation can lead to a chemical and structural change, especially polymeric sample materials. Many biological materials consist of or contain polysaccharides, which are long carbon-chain molecules. Only little is known about the influence of the ion-bombardment on

biological material, but some publications describe the influence of ion-implantation on polymers. The major influence is the breaking and formation of chemical bonds (Dlubek *et al.*, 2000; Červená *et al.*, 2002; Guenther *et al.*, 2002; Collwell *et al.*, 2003). Mainly covalent bonds are broken and radicals, unsaturated bonds and new additional aromatic, olefinic, carbonyl and hydroxyl groups are formed, which lead to cross linking, chain scission and to chemically reactive degradation products mainly H_2, CH_4, CO, CO_2 gases which are released (He *et al.*, 1998), and pyrolysis. All this leads to the formation of an amorphous and graphite like structure and with it to a change in the mechanical properties of the polymers.

The influence of high energy ions on polymers was investigated by Guenther *et al.* (2002). They investigated the change in hardness and Young's modulus of several polymers (polyimides and polyethersulfones) irradiated with a dose of 10^{16} B^+/cm^2 at an ion energy of 180 keV. After the irradiation they measured the hardness and Young's modulus using nanoindentation and they also found that the hardness and Young's modulus increased by a factor of six and ten, respectively. The fluences used in Chapter 1.6.4 were much higher, ranging from 10^{18} to 10^{19} Ga^+/cm^2 (ion energy of 30 keV) and the Ga^+ ions have a higher weight than the B^+ ions with Guenther *et al.* (2002) used. Our use of heavier ions and lower acceleration voltages seems to result in higher sputter yields at the samples surface and less ion implantation, which affects the mechanical properties, so that the changes in the mechanical properties (up to 22 %) are less dramatic when compared to those of Guenther *et al.* (2002).

1.8 Conclusions

The Focussed Ion Beam system, initially developed for imaging and micromachining of technical materials, can successfully be applied to the investigation of biological materials, as demonstrated in this thesis and in the literature published. The great advantage of the FIB system is its combination of high resolution microscopy (spatial resolution 6 nm) with a high depth of focus and the option for site-specific cutting (spatial resolution 10 nm). It is possible to micromachine certain structures, especially free standing features, with high accuracy, from a wide range of polymeric, biological and mineralised materials like insect cuticle, keratin, wood, dentin and enamel. High resolution images of the structures and cross-sections show the three dimensional geometry, which is advantageous for the investigation of interior structures like biological sensors or organs.

Conventional techniques for the exploration of such structures are light microscopy, TEM and SEM investigations, which require elaborate sample preparation methods like embedding and serial sectioning. In addition to artefacts, which are introduced during embedding, the major disadvantage of these methods is that they are not site-specific. It is necessary to make a set of slices in which the feature of interest is, hopefully, hit.

The micrographs taken with the FIB provide different information than the micrographs taken with a light microscope, TEM or SEM. In an optical microscope or a TEM only two dimensional images are possible. Additionally, the contrast in the FIB micrographs is a combination of topography and material contrast. This is advantageous for the investigation of composite structures. Different types of material appear separated. The advantage of optical microscopy is that different types of material can be stained to show structural and material differences. This is, however, more time consuming. Sample preparation for the FIB is comparatively straightforward. The only requirement is that the samples are at least air dry before they can be investigated in the FIB.

That the samples have to be dry mounted is the major disadvantage of the FIB for the investigation of biological materials. Drying biological materials causes artefacts like shrinking, the formation of cracks and a change in material properties. Artefacts can be reduced by the use of critical point drying, a method which is frequently used in the preparation of biological samples for the investigation in an SEM.

Another disadvantage is the redeposition of the sputtered material during milling, but it can be avoided by choosing advantageous aspect ratios, a stepwise milling process and the use of the gas enhanced etching, which uses a radical releasing precursor gas.

A third disadvantage is that the ion-bombardment leads to the implantation of gallium into the sample surface, which is associated with an energy transfer into the material. This energy leads to a rise of the local temperature, combined with a chemical and structural change of the material. For polymers and biological materials this local rise in temperature and the irradiation with the ions lead to cross linking and chain scission. Both have an influence on the mechanical properties of the exposed material. The temperature rise is significant, up to about 165 K (Ishitani and Kaga, 1995) in wood cell wall material for a typical beam current of 150 pA. This value even rises by a factor of 2 to 4 for cross-sections or pillar like structures, but due to the very low thermal conductivity of these materials the affected volume is thermally isolated from the surrounding material.

The investigations of the ion beam affected hardness and Young's modulus using the naoindentation technique have shown that the change in the mechanical properties is significant in a depth down to about 100 nm. Beyond this, the mechanical properties show no effect of the exposure with the gallium ions. TRIM simulations have shown that the maximum stopping range of the ions is about 73 nm Kapton®. We can conclude that the sample material is affected by the influence of the 30 keV Ga^+-ions (rise in temperature, change of the mechanical properties), but that the affected volume is very small. For samples bigger than 1 μm, these influences may be neglected.

1.9 References

Aubry C., Trigaud T., Moliton J.P. and Chiron D. (2002) "Polymer gratings achieved by focused ion beam" *Elsevier Synthetic Metals*, **127** (1-3), 307-311

Ballerini M., Milani M., Costato M., Squadrini F. and Turcu I.C.E. (1997) "Life science applications of focused ion beam (FIB)" *European Journal of Histochemistry* **41**, 89-90

Ballerini M., Milani M., Costato M., Turcu I.C.E. and Squadrini F. (1998) "Focused ion beam and life science applications: cell tomography and biomachining at ultrahigh resolution" *Proceedings of SPIE* **3260**, 221-230

Ballerini M., Milani M., Batani D. and Squadrini F. (2001) "Focused ion beam techniques for the analysis of biological samples: a revolution in ultramicroscopy?" *Proceedings of SPIE* **4261**, 92-104

Batani D., Masini A., Lora Lamia Donin C., Cortelli F., Previdi F., Dilani M., Faral B., Conte E., Moret M., Poletti G. and Pozzi A. (1998) "Characterisation of *saccharomyces cerevisiae* yeast cells" *Physica Medica* **XIV No. 4**, 151-157

Burkhardt C., Gnauck P., Wolburg H. and Nisch W. (2005) "Serial block-face sectioning and high resolution imaging of biological samples with a crossbeam FIB / FESEM microscope" *Abstract for the Dreiländertagung Microscopy Conference Davos 28.8-02.09.2005*

Červená J., Vacík J., Hnatowicz V., Macková A., Peřina V. and Fink D. (2002) "Decoration of radiation damages in polyimide implanted with rare gas ions" *Surface and Coatings Technology* **158-159**, 391-394

Chyr I. and Stechl A.J. (2001) "GaN focused ion beam micromachining with gas-assisted etching" *Journal of Vacuum Science and Technology* B **19(6)**, 2547-2550

Colwell J.M., Wentrup-Byrne E., Bell J.M. and Wielunski L.S. (2003) "A study of the chemical and physical effects of ion implantation of micro-porous and nonporous PTFE" *Surface and Coatings Technology* **168**, 216-222

Ding J.D., Meng Y.G. and Wen S.Z. (2001) "Specimen size effect on mechanical properties of polysilicon microcantilever beams measured by deflection using a nanoindenter" *Materials Sience and Engineering* B **83**, 42-47

Dinwoodie J. M. (2000) *Timber: Its nature and behaviour*, 2nd edition, E & FN Spon New York

Dlubek G., Börner F., Buchhold R., Sahre K., Krause-Rehberg R. and Eichhorn K.-J. (2000) "Damage-depth profiling of ion-irradiated polyimide films with a variable-energy positron beam" *Journal of Polymer Science: Part B: Polymer Physics* **38,** 3062-3069

Drobne D., Milani M., Zrimec A., Zrimec M.B., Tatti F. and Drašlar K. (2005) "Focused ion beam/scanning electron microscopy studies of *Porcellio scaber* (Isopoda, Crustacea) digestive gland epithelium cells" *Scanning* **27**, 30-34

Duane A.M. (1997) "Taxonomic investigations of palynomorphs from the Byers group (upper Jurassic – lower Cretaceous), livingston and snow islands, Antarctic Peninsula" *Palynology* **21**, 123-144

DuPont data sheets (2005) DuPont de Nemours S.A. Z.A. de Courtabouef 3 Av. Du Canada – B.P. 85 F-91943 Les Ulis Cedex A, France

fei 200xP manual (1996) *Focused ion beam workstation reference guide*, fei Company, 7451 NW Evergreen Parkway, Hillsboro, USA

Fu Y.Q., Bryan N.K.A., Shing O.N. and Hung N.P. (2000) "Influence of the redeposition effect for focused ion beam 3-D micromachining in silicon" *International Journal of Advanced Manufacturing and Technology* **16**, 877-880

Gere J.M. and Timoschenko S.P. (1984) *Mechanics of Materials*, second edition, PWS-Kent Publishing Company, Boston, USA

Giannuzzi L.A. and Stenie F.A. (1999) "A review of focused ion beam milling techniques for TEM specimen preparation" *Micron* **30**, 197-204

Gnatzy W. and Schmidt K. (1971) „Die Feinstruktur der Sinneshaare auf den Cerci von Gryllus Bimaculatus Deg. (Saltatoria, Gryllidae)" *Zeitschrift Zellforschung* **122**, 190-209

Gnauck P., Burkhardt C., Wolburg H. and Nisch W. (2005) "Investigation of the interface between biological cell tissue and hard substrate materials using cross beam technology" *Accepted in Microscopy and Microanalysis*

Goodfellow SARL, rue Solférion, F-59000 Lille, France (www.goodfellow.com → Material Properties)

Guenther M., Gerlach G., Suchaneck G., Sahre K., Eichhorn K.-J., Wolf B., Deineka A. and Jastrabik L. (2002) "Ion-beam induced chemical and structural modifications in polymers" *Surface and Coatings Technology* **158-159**, 108-113

Hayashi Y., Yaguchi T., Ito K. and Kamino T. (1998) "High-resolution electron microscopy of human enamel sections prepared with focused ion beam system" *Scanning* **20(3)**, 234-235

He D. and Bassim M. N. (1998) "Atomic force microscope study of crater formation in ion bombarded polymer" *Journal of Materials Science* **33(14)**, 3525-3528

Hoshi K., Ejire S., Probst W., Seybold V., Kamino T., Yaguchi T., Yamahira N. and Ozawa H. (2001) "Observation of human dentine by focused ion beam and energy-filtering transmission electron microscopy" *Journal of Microscopy* **201**, 44-49

Ishitani T., Hirose H. and Tsuboi H. (1995) "Focused ion beam digging of biological specimens" *Journal of Electron Microscopy* **44**, 110-114

Ishitani T. & Kaga H. (1995) "Calculation of local temperature rise in focused ion beam sample preparation" *Journal of Electron Microscopy* **44,** 331–336

Kanaya K., Muranaka Y., Yonehara K. and Adachi K. (1992) "Quantitative analysis of sputtering due to ion beam bombardment of solid and biological specimens in high resolution electron microscopy" *Micron and Microscopia Acta* **23(1/2)**, 45-64

Keil T. A. (1998) *The structure of integumental mechanoreceptors microscopic anatomy of invertebrates* Volume 11B Insecta pp. 385-404 Wiley-Liss, Inc, USA

Kim S.S., Kim S. J., Moon Y. D. and Lee Y. Moo (1994) "Thermal characteristics of chitin and hydroxypropyl chitin" *Polymer* **35 No. 15**, 3212-3216

Kumagai T., Shimozawa T. and Baba Y. (1998) "The shape of wind-receptor hairs of cricket and cockroach" *Journal of Comparative Physiology* **A 183**, 187-192

Langford R.M., Dale G., Hopkins P.J., Ewen P.J.S. and Petford-Long A.K. (2002) "Focused ion beam micromachining of three-dimensional structures and three-dimensional reconstruction to assess their shape", *Journal of Micromechanical Microengineering* **12**, 111-114

Larson D.J., Foord D.T., Petford-Long A.K., Anthony T.C., Rozdilsky I.M., Cerezo A. and Smith G.W.D. (1998) "Focused ion-beam milling for field-ion specimen preparation: preliminary investigations", *Ultramicroscopy* **75**, 147-159

Lewis S.M., Osborn J.S. and Sturad P.R. (1968) "Demonstration of an internal structure within the red Blood cell by ion etching and scanning electron microscopy" *Nature* **220**, 614-616

Lipp S., Frey L., Franz G., Demm E., Petersen S. and Ryssel H. (1995) "Local material removal by focused ion beam milling and etching" *Nuclear Instruments and Methods in Physics Research* B **106**, 630-635

Mackenzie J.M., Woodward T.H., Griffis D.P. and Russell P.E. (1993) *Nanosurgery Of Biological Specimens Using A Focused Ion Beam* Bailey G.W. and Rieder C.L. Eds., Proc. 51st Annual Meeting of the Microscopy Society of America Published by San Francisco Press, San Francisco, CA, USA

Melngailis J. (1987) "Critical review: Focused ion beam technology and applications" *Journal of Vacuum Science and Technology* B **5(2)**, 469-495

Milani M., Ballerini M. and Squadrini F. (2000) "Focused ion beam: moving towards nanobiotechnology" *Proceedings of SPIE* **3922**, 212-221

Milani M., Drobne D. and Zrimec A. (2005) "FIB in situ manipulation and imaging of biological samples" *Scanning* **27(2),** 60-61

Phaneuf M.W. (1999) "Applications of focused ion beam microscopy to materials science specimens" *Micron* **30**, 277-288

Rubanov S. and Munroe P.R. (2000) "Influence of the redeposition effect for focused ion beam 3-D micromachining in silicon", *International Journal of Advanced Manufactoring and Technolology* **16**, 877-880

Rubanov S. and Munroe P.R. (2001) "Investigation of the structure of damage layers in TEM samples prepared using a focused ion beam" *Journal of Materials Science Letters* **20**, 1181-1183

Seidel R., Private communication (2005) University of Reading, Centre for Biomimietics, Reading, United Kingdom

Stark T.J., Griffis D.P. and Russell P.E. (1996) "Characterization of resist profiles using water enhanced focused ion beam milling" *Journal of Vacuum Science and Technology* B **14 (6)**, 3990-3995

Suzuki H., Tanaka J. and Nagumo T. (2001) "Morphology of the marine diatom *Cocconeis Pseudomarginata* Gregory Var. *Intermedia* Grunow" *Diatom Research* **16 (1)**, 93-102

Van Meerbeek B., Conn Jr. L.J., Duke E.S., Schraub D. and Ghafghaichi F. (1995) "Demonstration of a focused ion-beam cross-sectioning technique for ultrastructural examination of resin-dentin interfaces" *Dental Materials* **11**, 87-92

Vasile M.J., Nassar R., Xie J. and Guo H. (1999) "Microfabrication techniques using focused ion beams and emergent applications" *Micron* **30**, 235-244

Vasile M.J., Xie J. and Nassar R. (1999) "Depth control of focused ion-beam milling from a numerical mode of the sputter process" *Journal of Vacuum Science and Technology* B **17(6)**, 3085-3090

Volkert C.A., Busch S., Heiland B. and Dehm G. (2004) "Transmission electron microscopy of fluorapatite-gelatine composite particles prepared using focused ion beam milling" *Journal of Microscopy* **214**, 208-212

Yonehara K., Baba N. and Kanaya K. (1989) "Application of ion-beam etching techniques to the fine structure of biological specimens as examined with a field emission SEM at low voltage" *Journal of Electron Microscopy Technique* **12**, 71-77

Yongqi F., Bryan N.K.A., Hung N.P. and Shing O.N. (2000) "Experimental study of three-dimensional microfabrication by focused ion beam technology" *Review of scientific Instruments* **71(2)**, 1006-1008

Young R.J., Dingle T., Robinson K. and Pugh P.J.A. (1993) "An application of scanned focused ion beam milling to studies on the internal morphology of small arthopods" *Journal of Microscopy* **172**, 81-88

Xu X., Della Ratta A.D., Sosonkina J. and Melngailis J. (1992) "Focused ion beam induced deposition and ion milling as a function of angle of ion incidence" *Journal of Vacuum Science and Technology* B **10(6)**, 2675-2680

Ziegler, J.F. and Biersack, J.P. (2004) TRIM, in SRIM 2003.26, (available fromhttp://www.srim.org/